UNIVERSIDADE
BEIRA INTERIOR

Plasmid DNA-loaded calcium phosphate functional nanocomplexes: innovative approach against cervical cancer

Versão final após defesa

Matilde Bogalheiro Costa

Dissertação para obtenção do Grau de Mestre em

Biotecnologia

2º ciclo de estudos

Orientador: Prof. Doutor Ângela Maria Almeida de Sousa

Co-orientador: Prof. Doutor Joana Filipa Abreu Pereira Valente

Co-orientador: Investigadora Doutorada Tatiana Marisa Fernandes Patrício

novembro de 2023

Declaração de Integridade

Eu, Matilde Bogalheiro Costa, que abaixo assino, estudante com o número de inscrição M11692 de/o Biotecnologia da Faculdade de Ciências, declaro ter desenvolvido o presente trabalho e elaborado o presente texto em total consonância com o **Código de Integridades da Universidade da Beira Interior**.

Mais concretamente afirmo não ter incorrido em qualquer das variedades de Fraude Académica, e que aqui declaro conhecer, que em particular atendi à exigida referenciação de frases, extratos, imagens e outras formas de trabalho intelectual, e assumindo assim na íntegra as responsabilidades da autoria.

Universidade da Beira Interior, Covilhã 29/11 /2023

Assinado por: **Matilde Bogalheiro Costa**
Num. de Identificação: 30312094
Data: 2023.11.29 19:13:36+00'00'

(assinatura conforme Cartão de Cidadão ou preferencialmente

assinatura digital no documento original se naquele mesmo formato)

“Basically, I have been compelled by curiosity”

- Mary Leaky

Acknowledgments

Completing this master's thesis has been a journey of both personal and academic growth and I am deeply grateful to the many individuals who have supported and inspired me along the way.

First and foremost, I extend my heartfelt gratitude to Professor Doctor Ângela Sousa, Professor Doctor Joana Valente, and to the Researcher Tatiana Patrício. Their expertise, suggestions, critical evaluation, and insightful guidance have been instrumental in shaping this research. Their willingness to invest time and effort in sharing their knowledge, discussing ideas, and providing constructive feedback has been invaluable.

I extend my gratitude to the University of Beira Interior, especially the Health Sciences Research Centre, and the Centre for Rapid and Sustainable Product Development of the Polytechnic of Leiria, for granting me access to its research facilities, equipment's, and available material. Furthermore, I would like to acknowledge Professor Lino Ferreira and Susana Soares from Biocant for the DLS analysis.

I also want to acknowledge the assistance and camaraderie of my fellow lab colleagues. The exchange of ideas, collaboration, and shared experiences have enriched my academic journey, and I am thankful for the friendships that have formed along the way. I would like to express my sincere appreciation and gratitude to Beatriz Carvalho for your outstanding contributions and support during our time working together. My special thanks to Dalinda Eusébio, Diana Gomes and Diana Pereira for helping me when I needed and teaching me the necessary lab techniques.

To new friends and old friends, I thank you! To my Salinha group, thank you for your guidance, ideas, and advices. Specially to Adriana, Carolina, and Ricardo, I cherish the time we spent together, and I am thankful for your friendship. A big thank you to João, Mafalda and Inês, whether through laughter, support, shared adventures, or quiet moments, you have been there, making my journey richer and more meaningful.

Finally, thank you to my family who have been a constant source of encouragement and motivation through this journey. I am thankful for their unwavering belief in me, their understanding in tough times and their joyous celebration of my achievements. To my parents, Cristina and José, my sister, Maria, my grandparents, Deolinda and Francisco and my aunt and cousin, Laura, and Salvador, thank you for always being there for me and providing the best possible.

Resumo

O cancro representa uma das principais causas de morte em todo o mundo. Até 2040, estimasse que o número de novos casos de cancro aumente para 29,5 milhões e o número de mortes associadas aumente para 16,4 milhões. Na maioria dos casos, a taxa de incidência tem aumentado nos países com maior esperança média de vida, nível de educação e qualidade de vida. No entanto, no caso do cancro do colo do útero, acontece o oposto, a sua incidência é maior em países menos desenvolvidos, devido à falta de consciencialização sobre a doença, programas de rastreio e procedimentos de tratamento eficazes, factos que levam a um diagnóstico tardio e, consequentemente, a taxas de sobrevivência baixas.

O vírus do papiloma humano (HPV), é um vírus sexualmente transmissível, e a principal causa da ocorrência do cancro do colo do útero. Cerca de 79 % dos casos diagnosticados são atribuídos às estirpes de maior risco, HPV-16 e HPV-18. A gravidade dos sintomas está associada à afinidade das oncoproteínas E6 e E7 pelas proteínas supressoras de tumores, p53, e proteína do retinoblastoma, pRb, respetivamente; uma vez que desregulam a expressão destas proteínas levando à invasão, proliferação e sobrevivência das células cancerígenas. Várias estratégias estão a ser desenvolvidas para detetar e prevenir esta doença, tais como vacinas contra o HPV. No entanto, em países menos desenvolvidos as medidas preventivas nem sempre funcionam, pelo que novas terapêuticas estão a ser desenvolvidas para o tratamento mais eficiente desta patologia.

A terapia génica tem sido amplamente explorada nos últimos tempos por permitir corrigir um determinado defeito genético ou até mesmo induzir a morte programada de uma célula anormal. Assim, o DNA plasmídico que codifica o gene da p53 representa uma abordagem promissora para combater o cancro do colo do útero. No entanto, o seu uso é limitado, uma vez que é facilmente degradado por vários agentes, sendo necessário um sistema de entrega para proteger, transportar e entregar o pDNA às células alvo. Nanopartículas de fosfato de cálcio apresentam benefícios uma vez que são compostas por iões que existem naturalmente no corpo humano e a sua degradação não implica consequências negativas.

Neste contexto, o foco principal do presente trabalho é o desenvolvimento de nanopartículas de fosfato de cálcio para encapsular pDNA e serem funcionalizadas com ácido fólico para uma entrega direcionada às células cancerígenas HPV positivas.

Inicialmente, as condições da formulação deste sistema de entrega foram otimizadas, resultando em sistemas com tamanhos de 76,34 ± 34,08 nm, com índice de polidispersividade (PdI) de 0,40 ± 0,09 e uma carga superficial de – 20,90 ± 0,90 mV. A inclusão do pDNA foi realizada através do método de adsorção, resultando num tamanho de 133,13 ± 58,12 nm, PdI de 0,65 ± 0,17 e uma carga superficial de – 23,70 ± 1,10 mV, com uma eficiência de encapsulação de aproximadamente 100 %.

Posteriormente, foi explorada a funcionalização com ácido fólico tendo sido escolhidas duas metodologias de formulação, a primeira consiste na adição do ácido fólico na solução precursora de cálcio (CaP-NP/FACa) e a segunda consiste na adição do ácido fólico por adsorção após a formulação (CaP-NP/FAAd). Estas formulações apresentaram uma eficiência de *loading* deste ligando de aproximadamente 70 e 92 %, respetivamente. Após a inclusão de pDNA nos sistemas, a formulação CaP-NP/pDNA/FAAd apresentou uma eficiência de aproximadamente 100 % para a encapsulação de pDNA e aproximadamente 99,6 % para o ácido fólico, com um tamanho de 112,63 ± 19,81 nm, PdI de 0,50 ± 0,22 e uma carga superficial de – 27,40 ± 0,69 mV. A formulação CaP-NP/pDNA/FACa apresentou uma eficiência de encapsulação de pDNA de aproximadamente 100 % e uma eficiência de aproximadamente 73 % para a funcionalização com ácido fólico, com um tamanho de 110,42 ± 65,71 nm, PdI de 0,50 ± 0,07 e uma carga superficial de – 22,20 ± 0,60 mV.

De forma geral, os ensaios *in vitro* não mostraram citotoxicidade inerente às CaP-NPs. Somente foi observada a diminuição da viabilidade celular quando foram aplicadas concentrações elevadas (500 e 1000 µg/mL) destes sistemas. Os sistemas de entrega não afetaram a viabilidade das células saudáveis, mas diminuíram a viabilidade das células cancerígenas. A internalização das nanopartículas foi verificada através de microscopia confocal, tendo se observado elevada internalização em ambas as linhas celulares, com particular incidência nas células cancerígenas. As formulações de pDNA com inclusão do ácido fólico na solução de cálcio (CaP-NP/pDNA/FACa) e adsorvido após a formulação (CaP-NP/pDNA/FAAd) parecem ter melhor capacidade de internalização. A avaliação por PCR parece apresentar um nível superior de transcritos de p53 na linha celular cancerígena quando a transfeção foi realizada com CaP-NP/pDNA e com CaP-NP/pDNA/FACa.

De modo geral, o presente trabalho demonstrou que os sistemas CaP-NP apresentam o efeito terapêutico desejado e mostram-se promissores para o tratamento do cancro do colo do útero.

Palavras-chave

Ácido Fólico; Cancro do Colo do Útero; DNA Plasmídico; HPV; Nanopartículas de Fosfato de Cálcio; p53

Abstract

Cancer is among the leading causes of death worldwide. By 2040 it is expected that the number of new cancer cases will rise to 29.5 million and the number of cervical cancer-related deaths to 16.4 million. Generally, cancer incidence rate increases in countries with highest life expectancy, education level and standard of living. However, for cervical cancer the reverse happens, its incidence is higher in less developed countries, due to the lack of proper awareness, screening programs, inaccessibility to proper diagnosis and efficient treatment procedures, these facts lead to a late diagnosis and consequently low survival rates.

Human Papillomavirus (HPV), a highly sexually transmissible virus, is the main agent in cervical cancer. Around 79 % of the diagnosed causes are attributed to HPV-16 and -18. The severity of symptoms is usually associated with the affinity presented by oncoproteins E6 and E7 within each HPV type toward the target protein, p53, a tumour suppressor, and pRb, a retinoblastoma protein, respectively. Thus, the deregulation of these proteins' expression leads to invasion, proliferation, and survival of cancer cells. A plethora of strategies are being developed to detect and prevent the disease, with anti-HPV vaccines being at the front. However, in less developed countries, with poor health resources, the preventative measures do not always work, and new therapies are being developed to treat this type of cancer.

Gene therapy has been increasingly used since it allows the correction of a genetic effect while also facilitating for an induced cell death. Thus, plasmid DNA that encodes the p53 gene can be a promising approach to combat cervical cancer. However, pDNA use is limited since it is easily degraded by various agents, so a delivery system is needed to carry pDNA to the target cells. Calcium phosphate nanoparticle are promising delivery systems since they are composed of ions that naturally exist in the human body, and its degradation does not entail negative consequences for the patient.

In this context, the present work's focus is the development of plasmid DNA-loaded calcium phosphate nanoparticles and further functionalization with folic acid for a targeted delivery to HPV positive cancer cells.

Initially, the delivery system formulation was optimized resulting in delivery systems presenting a size of 76.34 ± 34.08 nm, with a polydispersity index (PdI) of 0.40 ± 0.09 and a surface charge of – 20.90 ± 0.90 mV. pDNA inclusion was performed through an adsorption approach yielding a size of 133.13 ± 58.12 nm, PdI of 0.65 ± 0.17 and a surface

charge of – 23.70 ± 1.10 mV with an encapsulation efficiency of approximately 100 %. Folic acid loading was investigated, and two methods were chosen, firstly when folic acid is added in the precursor calcium solution (CaP-NP/FACa) and also when folic acid is added through adsorption (CaP-NP/FAAd), which exhibited a folic acid loading efficiency of approximately 92 and 70 %, respectively. The CaP-NP/pDNA/FAAd achieved an efficiency of approximately 100 % for pDNA encapsulation and approximately 99.6 % for folic acid loading, with a size of 112.63 ± 19.81 nm, PdI of 0.50 ± 0.22 and a surface charge of – 27.40 ± 0.69 mV. The CaP-NP/pDNA/FACa presented an encapsulation efficiency of pDNA in the nanoparticles of 100 % and an efficiency of approximately 73 % for the loading of folic acid, with a size of 110.42 ± 65.71 nm, PdI of 0.50 ± 0.07 and a charge of – 22.20 ± 0.60 mV.

Overall, the *in vitro* assays showed no inherent cytotoxicity for the CaP-NPs, with viability reduction only in higher concentrations (500 and 1000 μg/mL). The delivery systems did not affect the healthy cells viability but decreased the viability in the cancer cell line. Cell internalization was evaluated through confocal microscopy, which showed significant uptake in both cell lines. The formulations presenting pDNA and folic acid, in the calcium solution (CaP-NP/pDNA/FACa) and adsorbed after the nanoparticle formulation (CaP-NP/pDNA/FAAd), presented high accumulation in cancer cells. PCR evaluation seems to present increased expression values of p53 when the cancer cell line was transfected with both CaP-NP/pDNA and CaP-NP/pDNA/FACa.

The present work demonstrated that CaP-NPs, loaded with pDNA and modified with folic acid, show a therapeutic effect, and represents a promising treatment for cervical cancer.

Keywords

Calcium Phosphate Nanoparticles; Cervical Cancer; Folic Acid; HPV; p53; Plasmid DNA

Index

List of Figures

List of Tables

List of Abbreviations

AAV	Adeno-Associated Virus
AC	Affinity Chromatography
ACP	Amorphous Calcium Phosphate
A_E	Early pA
AEC	Anion-Exchange Chromatography
A_L	Late pA
ASON	Anti-sense Oligonucleotide
CaP-NP	Calcium Phosphate Nanoparticle
cDNA	Complementary DNA
CNT	Carbon Nanotube
CR1	Conserved Region 1
CR2	Conserved Region 2
DCP	Dicalcium Phosphate
DEPC	Diethylpyrocarbonate
DLS	Dynamic Light Scattering
DMEM-F12	Dulbecco's Modified Eagle's Medium with Ham's F-12 Nutrient Mixture
DNA	Deoxyribonucleic Acid
dNTP	Deoxynucleotide
dsDNA	Double-stranded DNA
E	Early Region
E. coli	*Escherichia coli*
E6AP	E6 associated protein
EMT	Epithelial-to-Mesenchymal Transition
EPR	Enhanced Permeability and Retention
FBS	Foetal Bovine Serum
FITC	Fluorescein Isothiocyanate
FTIR	Fourier Transform Infrared Spectroscopy
FW	Forward
gDNA	Genomic DNA
HA	Hydroxyapatite
HIC	Hydrophobic Interaction Chromatography
HPV	Human Papillomavirus
L	Late Region

LB	Luria-Bertani
LCR	Long Control Region
MCP	Monocalcium Phosphate
MCPM	Monocalcium Phosphate Monohydrate
MRI	Magnetic Resonance Imaging
mRNA	Messenger RNA
NCCR	Non-coding Region
NP	Nanoparticle
oc	Open-circular
OCP	Octacalcium Phosphate
$OD_{600\ nm}$	Optic density at 600 nm
ori	Origin of Replication
pA	Polyadenylation
PBS	Phosphate Buffered Solution
PCR	Polymerase Chain Reaction
PDI	Polydispersity Index
pDNA	Plasmid DNA
PEG	Polyethylene Glycol
pFAR	Plasmid Free-of-Antibiotic Resistance
PNP	Polymeric Nanoparticle
pRb	Retinoblastoma Protein
RES	Reticuloendothelial System
RNA	Ribonucleic Acid
RPLC	Reversed-Phase Liquid Chromatography
RPM	Revolutions per minute
RT-PCR	Reverse Transcription-Polymerase Chain Reaction
RV	Reverse
sc	Supercoiled
SD	Standard Deviation
SEC	Size-Exclusion Chromatography
ssDNA	Single-stranded DNA
TB	Terrific Broth
TCP	Tricalcium Phosphate
TME	Tumour Microenvironment
TTCP	Tetracalcium Phosphate
URR	Upstream Regulatory Region
UV	Ultraviolet

Chapter 1 - Introduction

1.1 Cervical Cancer

Cervical cancer ranks among the leading causes of death in women and is the fourth most prevalent female cancer worldwide [1]. Every year, approximately 500,000 women are diagnosed, and tragically, nearly 250,000 lose their lives due to this disease [2]. Projections indicate that by 2030, the death toll will surpass 474,000, highlighting the immense global burden of this illness [1]. The single most important etiological factor of cervical cancer is infection by high-risk Human Papillomavirus (HPV), affecting an estimated 291 million women globally [3]. Nearly 85 % of deaths related to cervical cancer come from low or developing countries, where the mortality rate is eighteen times higher compared to developed nations. This stark disparity is primarily attributed to insufficient education and awareness, inadequate screening programs, and limited access to proper diagnosis and effective treatments in developing regions [4].

1.1.1 HPV Infection

Around 90 % of cervical cancer cases can be attributed to prior infections with HPV [5]. HPV is a member of the Papillomaviridae family and is classified into five genera: alpha (α), beta (β), gamma (γ), mu (μ), and nu (ν). Among these, the α-papillomavirus group is further categorized into low-risk and high-risk types. The low-risk types typically lead to benign lesions, while the high-risk types have been linked to the development of malignancies in anogenital and head-and-neck regions. Notably, two specific strains, HPV-16 and HPV-18, are responsible for approximately 80 % of cervical cancer cases worldwide [6].

HPV is categorized as a small, non-enveloped, circular, double-stranded DNA virus, with a diameter measuring 50-55 nm. Its genome spans approximately 8,000 base pairs and is divided into three sections: the early gene-coding region (E), the late gene-coding region (L), and the long control region (LCR), also referred to as the non-coding region (NCCR) or upstream regulatory region (URR) [7, 8]. These gene segments are divided by two polyadenylation (pA) sites, early pA (A_E) and late pA (A_L). The 5’ end begins with the E region, which has six open reading frames, E1, E2, E4, E5, E6 and E7. E1 and E2 play roles in regulating early proteins' transcription and viral genome replication. E4 influences the structure of infected epithelial cells' cytoskeleton to facilitate virion release. E5, E6, and E7 are responsible for cellular transformation, leading to oncogenesis. E5 aids in keratinocyte differentiation and immune evasion in later stages, while E6 and E7

control various cellular checkpoints, contributing to the development of cancer hallmarks [1, 7, 9]. These oncoproteins repress tumour suppressors p53 and retinoblastoma protein (pRb), disrupting the activation of apoptotic pathways and promoting cell proliferation. The L region is divided into two parts, L1, which encodes a major viral capsid protein, and L2, which encodes a minor viral capsid structure. On the other hand, the LCR does not contain any protein-coding sequence but holds the origin of replication and numerous binding sites for transcription factors [1, 7]. Figure 1 and Table 1 represent the HPV genome structure.

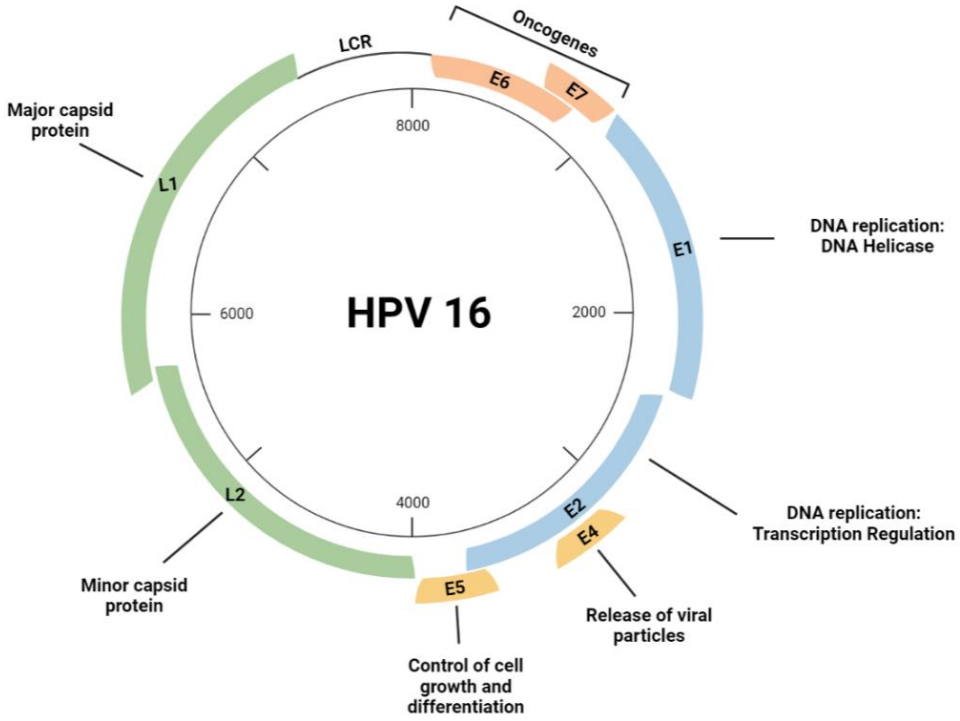

Figure 1 – Structure and organization of HPV-16 genome. Adapted from [7, 10]

Table 1 – Major role and activity of the genes in HPV. Adapted from [1, 7]

Genes	Activity
L1	Major capsid protein
L2	Minor capsid protein, recruits L1 and helps in virus assembly
E1	Replication of viral genome and its maintenance; ATP-dependent DNA helicase
E2	Initiation of viral DNA replication; regulation of transcription of E6 and E7 and of cellular gene expression
E4	Release of viral particles; remodels cytokeratin network; virion assembly
E5	Enhances growth factor signalling pathways
E6	Inhibits p53 and causes loss in cell cycle regulation; regulates cell shape, polarity, mobility, and signalling
E7	pRb mediated deregulation of cell cycle; controls centrosome duplication

1.1.1.1 Viral Life Cycle

The life cycle of HPV follows a biphasic pattern, encompassing both viral maintenance and amplification stages [11]. The viral infections initiate when a viral particle infects cells located in the basal layer of stratified squamous epithelia. This infection occurs only after the infected cell has undergone mitosis, and one of the daughter cells resulting from the division begins to synthesize new virions. As a consequence of microwounds, these basal cells become exposed and stand as the sole proliferating cells in normal epithelia. In contrast, the differentiated cells in the suprabasal layers have exited the cell cycle. Meanwhile, the suprabasal cells continue to be active in the cell cycle during the process of differentiation. Among this group of cells, a subset re-enters the S phase in the upper epithelial layers, engaging in a process known as amplification. During amplification, these cells replicate the HPV genome [12].

In the initial amplification phase of viral replication, proteins E1 and E2 play crucial roles, but once the copy number stabilizes, they can become dispensable for episomal maintenance-replication [13]. The early expression of the E2 viral transcription factor is essential for proper regulation of the viral early promoter. This regulation directs the expression of the E6 and E7 regulatory proteins, which are vital for the continued survival of HPV-infected cells. Moreover, these proteins exhibit pleiotropic functions, including transmembrane signalling, regulation of the cell cycle, transformation of established cells and regulation of chromosomal stability, these oncoproteins play a crucial role in malignant conversion. E2 forms a homodimer that can bind to four palindromic sites in the LCR, among these sites, three of them are required for E1-activated viral replication. E2 binds E1, and this complex acts as a dimer of hexamers, subsequently, it attaches to the viral origin of replication, facilitating the recruitment of the cellular DNA replication machinery. Notably, Brd4, facilitated by E2, is the most extensively studied anchor for HPV genomes to cellular chromosomes. However, under specific circumstances, the E1-E2 complex alone might be adequate for HPVs to position themselves onto cellular chromosomes [14, 15].

Upon infection, viral proteins are expressed at low levels within the infected basal cells, likely to evade triggering a local immune response. E2 plays a crucial role in this process by altering the chromatin structure and transcriptionally repressing the P97 promoter. Consequently, E2 prevents transcription factors from accessing the promoter, effectively suppressing its activity. As a result of these mechanisms, HPV can successfully sustain the state of infection in the epithelial cells for a significant duration [13, 14].

1.1.1.2 E6 and E7 Oncoproteins

The early gene products of papillomavirus, E6 and E7 function as oncoproteins, promoting uncontrolled cell proliferation, angiogenesis, invasion, metastasis, and unrestricted telomerase activity [7]. In HPV associated cancers, the continued expression of E6 and E7 sustains the constant expression of cancer phenotype [16]. Furthermore, the expression of biomarkers influenced by E6 and E7 was observed to decline in the upper epithelial layers, highlighting the crucial role of these proteins in the early phase of viral replication [14].

High risk HPV E6 is a short protein, comprising approximately 150 amino acids. Through Nuclear Magnetic Resonance the structure of this oncoprotein has been elucidated. It consists of zinc finger domains in its N and C termini, each one separated by a short linker region. Following the C-terminal zinc finger is a short PDZ-binding motif that facilitates interactions with PDZ domain-containing proteins [11].

PDZ domains are present in numerous proteins that oversee various biological pathways, such as cellular proliferation and polarity. Through this domain, the HPV E6 has the potential to affect a range of pathways, in viral propagation and HPV-associated oncogenesis. Recent work has demonstrated that this motif is required for induction of epithelial hyperplasia and cooperates with RAS to promote anchorage-independent growth [11].

High-risk HPV E6 directly binds to E6AP, a cellular E3 ubiquitin ligase encoded by the UBE3A gene, via its zinc finger domain. This binding alters the substrate specificity of the E6AP, leading to its stable association and polyubiquitylation of p53, which induces p53 degradation by the 26S proteasome [17]. Furthermore, HPV E6 also has a prominent function in the proteolytic inactivation of certain pro-apoptotic factors, such as Bak and Bcl-2. The Bcl-2 family of proteins critically regulates mitochondrial integrity and mitochondria-initiated apoptosis. Bak plays a key role in the apoptosis of several cell types. It has been found that increased levels of Bcl-2 and decreased Bak expression indicates a shift in the balance and favour of anti-apoptotic activity [15].

Another primary function of HPV E6 is the ability to activate telomerase, a ribonucleoprotein responsible for maintaining telomere length and preventing cellular senescence by adding repetitive sequences to the chromosome ends. This activation process is distinct from E6AP and p53 degradation. Instead, it involves a complex series of transactivation events, including interactions with Myc and the knockdown of the nuclear transcription factor NFX1-91 [11].

HPV E7 was the first oncogene to be discovered, among all the HPV oncogenes [7]. Structurally HPV E7 proteins contain approximately 100 amino acids [18]. HPV E7 can be divided into three regions, conserved region 1 (CR1), conserved region 2 (CR2) and the C-terminal region containing two zinc finger domains [19]. A small portion of CR1 and nearly the entire CR2 from the amino terminal holds sequence similarity with adenovirus E1A protein and large T antigen of SV40. The CR3 region follows a poorly conserved sequence in the CR2 domain. This conserved region at the carboxyl terminus encodes for a zinc finger domain with two CXXC motifs. This domain is responsible for zinc-dependent dimerization and facilitates E7's interaction with cellular proteins involved in cell cycle regulation and apoptosis [7].

Furthermore, one of the notable characteristics of HPV E7 is its ability to interact with the pRb through its LXCXE motif in CR2. This interaction leads to the inactivation of pRb, causing the release of E2F-responsive genes necessary for cell-cycle progression. As a result, genes such as cyclin E, cyclin A, and $p16^{INK4A}$ are transcribed, forcing the cells to go through premature S-phase entry [7, 19]. HPV E7 also interacts with other pocket proteins, such as p107 and p130, which are negative cell cycle regulators involved in the G_1 to S phase and G_2 to M phase. This interaction results in enhanced phosphorylation and degradation [14, 15]. Furthermore, the E7 expression early in the infection activates the G_1 to S-phase checkpoint in keratinocytes that would normally undergo terminal differentiation, consequently the number of epithelial cells in active DNA replication increases [14].

High-risk HPV E7 proteins contribute to an increased occurrence of mitotic aberrations through multiple mechanisms. Firstly, E7 expression triggers the aberrant synthesis of centrosomes, which forms the mitotic spindle poles. As a result, daughter cells arising from such aberrant and multipolar cell divisions end up with abnormal chromosome numbers. This condition is known as aneuploidy, which is the most frequent manifestation of genomic instability in solid tumours, including cervical cancers. In addition, HPV E7 also increases the incidence of unrepaired double strand DNA breaks in cells, which can lead to chromosomal fusion and translocations. Other mitotic abnormalities, include defects in chromosome alignment during metaphase [8].

Moreover, both E6 and E7 contribute to HPV-infected cells obtaining nutrition and oxygen from the surrounding tissues by regulating the expressions and activities of angiogenesis inducers and inhibitors. Additionally, both oncogenes have been found to induce the epithelial-to-mesenchymal transition (EMT), a process required for the tumour cells to invade the bloodstream and metastasize at other places in the body [7].

1.1.1.3 p53

The p53 protein is a nuclear phosphoprotein, comprised of 393 amino acids that fall into three functional domains, which are, a NH_2-terminal acidic transactivation domain, a DNA-binding domain, and an oligomerization domain [20, 21]. The DNA-binding domain plays a crucial role in the cellular stress response, as it facilitates the transactivation of target genes, leading to cell cycle arrest or apoptosis. Additionally, functional p53 forms a homo-tetramer, which is mediated by the oligomerization domain [21].

In addition to the functional domains, p53 has two structural domains, a proline-rich regulatory domain, and a C-terminal domain. The proline rich domain is associated with pro-apoptotic function of p53 since the deletion of this domain leads to a complete loss of pro apoptotic activity. Furthermore, the C-terminal domain participates in the regulation of DNA-binding [21, 22].

Under normal physiological conditions, p53 functions as a "guardian" to maintain genome stability and normal cellular processes [20]. Under normal conditions, it is expressed at an extremely low level, which is caused by proteasomal degradation mediated largely by RING-finger type E3 ubiquitin ligase MDM2. However, when DNA damage occurs, post-translational modifications such as phosphorylation and acetylation trigger p53 to accumulate in the cell nucleus. These chemical modifications alter p53 from a latent to active state. In its functionally active state, p53 transactivates a specific set of target genes, leading to cell cycle arrest and/or apoptosis, depending on the extent and nature of the DNA damage. When DNA damage is repairable, the p53-mediated cell cycle arrest allows cells to mend the damaged DNA, after which they re-enter the cell cycle. Conversely, if the DNA damage is irreparable, p53 exerts its pro-apoptotic function, preventing the transmission of damaged DNA to the daughter cells and thereby maintaining genomic integrity [21].

Approximately 50 % of human cancers harbour loss-of-function mutations in the p53 gene [21]. Of all reported mutations, 75 % are missense and 80 % of them occur within the sequence responsible for encoding the DNA-binding domain of the protein [22]. Consequently, mutant p53 lacks the sequence-specific transactivation ability, which is tightly linked to its pro-apoptotic function. Additionally, while p53 has a short life span, around 20 min, mutant p53 has a prolonged half-live, ranging from 2 to 12 h, with an oncogenic potential [21].

1.2 Gene Therapy

Cancer therapy worldwide primarily revolves around surgery, chemotherapy, and radiotherapy. Despite their widespread use, these methods are not always entirely effective, and cancer progression can sometimes remain uncontrolled. As a result, there is growing interest in gene therapy as a potential alternative approach to block cancer [23].

Gene therapy involves the use of nucleic acids to repair, replace, or regulate genes with to prevent or treat a disease [24]. The fundamental principle of gene therapy is to address acquired or inherited diseases by correcting their underlying genetic causes. This can be achieved by either replacing faulty genes with healthy ones or by providing the missing genes that are essential for normal cellular function [25].

Gene therapy employs several types of genetic material, including double-stranded DNA (dsDNA), single-stranded DNA (ssDNA), plasmid DNA (pDNA), and anti-sense oligonucleotides (ASON). However, due to the hydrophilic poly anionic nature of these molecules, they are sensitive to nuclease degradation and cannot passively penetrate the cell membrane. Therefore, they need to be associated with a delivery system or vector that can transport them to the targeted cell, protecting them from degradation [25]. Gene therapy vectors are broadly categorized as viral or non-viral [24]. Figure 2 provides an overview of the biotechnological processes required for the delivery of gene therapy.

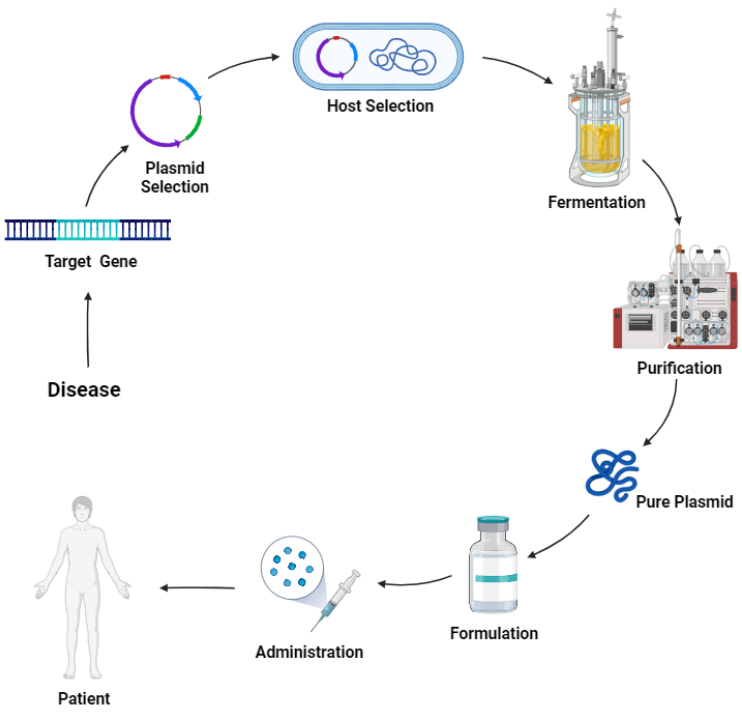

Figure 2 – Overview of gene therapy production steps. Adapted from [26].

In 2003, China became the first nation to authorize a gene therapy-based product for clinical use. This pioneering product, *Gendicine™*, is an adenoviral vector created by *SiBiono Gene Tech Co.*, which replaces the E1 gene with a human p53 cDNA [27]. By January 2006, there were approximately 1020 authorized gene therapy clinical trials conducted globally, with 66 % of these trials focused on cancer treatment. Among these clinical investigations, 58 trials employed a recombinant adenovirus expressing the human p53 tumour suppressor gene for cancer treatment [28].

In the year 2022, a total of 3685 gene therapy clinical trials were conducted, with a majority falling under phase I trials. Adenovirus continued to be the most widely used type of vector, while plasmid DNA ranked third with a usage rate of 13.1 %. Furthermore, p53 served as the therapeutic agent in 80 clinical trials [29]. Figure 3 illustrates the ongoing clinical trials.

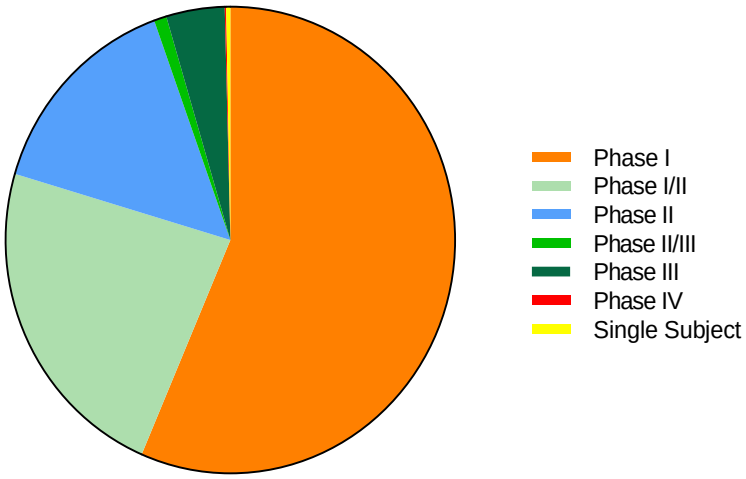

Figure 3 – Different phases of ongoing clinical trials (adapted from https://a873679.fmphost.com/fmi/webd/GTCT, accessed on 11 January 2023).

1.2.1 pDNA

Plasmids, the molecular tool that is most frequently employed for DNA alteration, transfer, and gene expression, have been crucial in the development of biotechnology during the past 50 years [30].

Plasmid vectors are small circular, double-stranded DNA molecules capable of replicating in bacterial host cells [31, 32]. Their size ranges from 0.8 to 10 kbp and the ability for transgene DNA is almost unrestricted [32]. Due to the compact phosphate groups in their backbone, plasmid DNA (pDNA) exhibits strong polyanionic properties [33]. Archae, bacteria, and some yeast contain this form of extrachromosomal DNA, it has at least one origin of replication (ori), where plasmid replication begins without first replicating chromosomal DNA [30]. An *ori* allows plasmids to deliver therapeutic sequences to also transfer into and replicate in other bacteria. Additionally, plasmids encode genes for selection of plasmid-harbouring bacteria. However, the use of antibiotic and resistance genes is discouraged by regulating agencies because of the risk of transfer and replication of resistance genes to bacteria in human microbiome or even the environment. Furthermore, the residual that remain from vector production may trigger an immune reaction or even resistance to certain antibiotics. To counter this disadvantage a new antibiotic-free selection system, such as plasmid Free-of-Antibiotic Resistance (pFAR) or RNA OUT, has been designed to increase biosafety [24, 32].

Thus, a plasmid must possess three essential features, an origin of replication, the presence of a selectable marker and a cloning or restriction enzyme cleavage site, where the foreign/therapeutic DNA is inserted (Figure 4) [31].

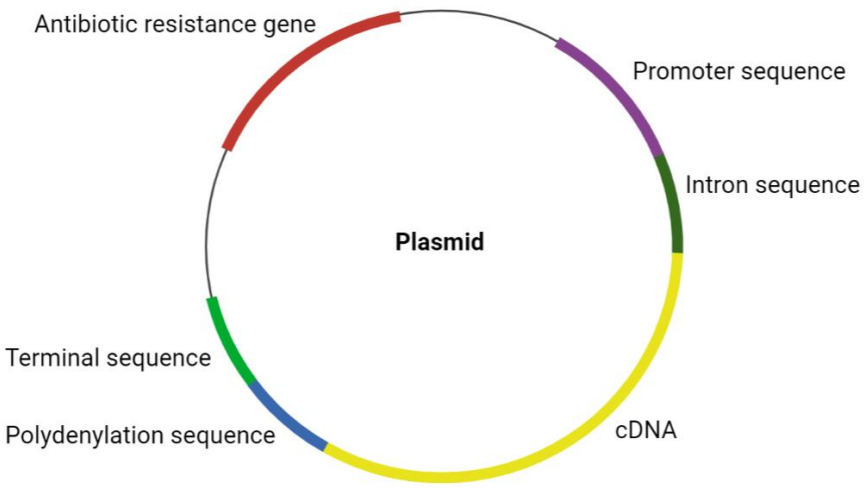

Figure 4 – Plasmid DNA construction. Adapted from [33].

pDNA presents five different conformations, each of them exhibits distinct size and therefore heterogenous speed in electrophoresis. The isoforms can be open-circular (oc), relaxed circular, linear, supercoiled (sc) and supercoiled denatured. The oc pDNA is circular and despite being double-stranded, the circular pDNA is relaxed because of an enzymatic action. The linear pDNA is cut double-stranded pDNA which has free ends. Sc pDNA is a dense conformation and consists of a double strand with the normal twist and shape. Finally, because of the unpaired sections in the helix, sc denatured pDNA is comparable to sc pDNA but less dense [34]. The sc isoform is considered the physiologically active conformation and is the most favourable for therapeutic use due to its outstanding stability and antigenicity [34, 35]. It is interesting to note that sc pDNA has a small hydrodynamic size, which may be the cause of its high intracellular mobility through entangled and cross-linked composite networks of actin and microtubules [36].

The process development for the manufacture of plasmid DNA typically begins on a small scale, with the construction and selection of a suitable expression vector and host, followed by the optimization of the fermentation conditions (upstream processing), cell growth and finally the isolation and purification steps (downstream processing). Upstream processing, fermentation and downstream processing are three steps of process development, which are interconnected and cannot be treated separately [37]. The key focus when developing a fermentation method is to maximize the volumetric yield of supercoiled plasmid as well as the specific yield of plasmid. Smaller and cost-effective fermentations are achieved by volumetric yield optimization, while downstream processing benefits from specific yield optimization by increasing plasmid purity. Furthermore, media composition impacts plasmid quality and yield, a balanced medium with sufficient levels of nutrients required for energy, biomass and cell maintenance is necessary for high cell density [38].

Following fermentation, a series of unit operations must be established to achieve highly purified plasmid DNA by removing all impurities present in the lysate [37, 38]. However, plasmid isolation typically incurs significant manufacturing costs. This high cost is primarily attributed to two factors. Firstly, plasmid DNA constitutes only a small fraction of the cell mass generated by fermentation. Secondly, separating plasmid from host nucleic acids poses a challenge. Therefore, the key goal is to develop a process that optimizes yield, purity, and safety while simultaneously minimizing expenses [38]. The approach involves choosing and integrating appropriate purification operations in two distinct stages. During the first stage (clarification and concentration), which occurs after the lysis process, high-volumetric-capacity and low-resolution operations are employed to eliminate cell debris and structurally unrelated impurities like proteins and low

molecular weight nucleic acids, these steps prepare the plasmid extract for the subsequent purification step. In the second stage, chromatography is utilized to isolate supercoiled plasmid DNA from structurally similar impurities such as relaxed and denatured plasmid DNA, genomic DNA (gDNA), high molecular weight RNA, and endotoxins [37].

To further elaborate, several studies have shown that within *E. coli* lysates, only 3 % of the total content is comprised of pDNA. In comparison, proteins make up a significantly larger portion at 55 %, while RNA accounts for 21 % [30]. During the clarification step, the presence of high molecular weight RNA is a concern. Typically, 'salting out' is utilized to remove the proteins that remain in the lysates by employing high concentrations of chaotropic salts. Some chaotropic salts, like ammonium acetate, ammonium sulfate and lithium chloride, offer the additional advantage of precipitating high molecular weight RNA and proteins together. After the clarification step, the pDNA is frequently concentrated using polyethylene glycol (PEG) precipitation to further eliminate small nucleic acids and decrease the volume of process streams before chromatographic purification [37]. Tangential flow filtration and aqueous two-phase partitioning can also be employed for concentrating and eliminating impurities from plasmid DNA preparations before chromatography [39].

Plasmid DNA purification poses unique challenges that are not typically encountered in purifying other biological molecules. These challenges are primarily related to the structural characteristics of plasmid DNA, such as its size, shape, and conformation, as well as the rheological properties (such as viscosity) of the lysates and process streams. Additionally, the presence of impurities with similar properties can complicate the purification process. The main objective is to quickly capture, concentrate, and purify sc pDNA in order to achieve high throughput and maximize product yield while minimizing product degradation [39]. The chemical composition of chromatographic supports plays a crucial role in determining the preferential interactions with the target molecule, enabling its retention while undesirable molecules are eluted [40]. The decision to employ one or multiple chromatographic methods with varying selectivity relies on the type and spread of residual impurities and contaminants, along with the projected plasmid yield [39]. Several chromatographic techniques, including size-exclusion (SEC), anion-exchange (AEC), hydrophobic interaction (HIC), reversed-phase (RPLC) and affinity (AC), have been incorporated into numerous therapeutic pDNA manufacturing processes either separately or in combination (Table 2) [41].

Table 2 - Chromatography techniques to purify pDNA. Adapted from [39–44].

Chromatographic Approach	Purification Principle	Advantages	Disadvantages
SEC	The reduction of the plasmid hydrodynamic radius due to supercoiling allows for its selective separation	Allows separation from RNA, oligonucleotides, endotoxins, and salts; Ideally used as a finishing step.	Limited capacity and selectivity
AEC	Based on the interaction between the negatively charged phosphate groups on the pDNA backbone and the positively charged groups on the stationary phase	Ideal to capture and concentrate plasmid DNA; Rapid and simple	Poor selectivity, leads to co-elution of impurities; Low capacity.
HIC	Explores the differences in hydrophobicity between pDNA, single-stranded nucleic acid impurities and endotoxins	Allows separation from RNA, oligonucleotides, endotoxins, and salts; High recovery percentage	Purified pDNA can be eluted in high salt or in the flow through and diluted
RPLC	Based upon the interaction of hydrophobic regions of molecules with non-polar immobilized ligands	Separates pDNA from contaminants, and other isoforms	Can lead to loss of pDNA integrity
AC	Explores the highly selective reversible interactions between the ligand and the substrate	High selectivity, specificity and efficacy	Expensive; Low versatility

1.2.2 Viral Vectors

A diverse array of viral vectors has been developed, offering delivery systems for both permanent or long-term expression and transient short-term expression [45]. Viral vectors are widely used due to their inherent ability to enter cells and transfer genetic information for therapeutic purposes [24]. Additionally, it is an effective form of gene delivery because of the virus structure preventing degradation via liposome [46]. To date, viral vectors are most often used to transfer genes, due to their high transfection efficiency *in vivo*. In truth, viruses have evolved over time to successfully infect a variety of cells with their genetic cargo. These viruses are simple to modify to deliver the desired genetic cargo into target cells. As a result, most clinical trials and approved gene therapy for human use are based in viral vectors, some examples include *Luxturna*, *Zolgensa*, *Oncorine* and *Imlygic* [47]. However, these approaches present some drawbacks, such as, causing a potential acute immune response, the size limit of the gene to be delivered and their production in large quantities is exceedingly difficult and too expensive [25].

The most used viruses as carrier vectors in gene therapy include retroviruses, adenoviruses, adeno-associated virus (AAV), simple herpes virus and lentiviruses (Table 3) [25, 45]. Retroviral vectors, which are designed for insertion into the genome, carry a substantial risk of gene disruption. AVV vectors have a lower but still existent risk of insertional mutagenesis. Adenoviral vectors are maintained episomally, which can cause toxicity and immunogenicity. In all these families of viral vectors the same serotype of construct cannot be delivered repeatedly to the same patient because it will elicit an immune response, rendering the subsequent deliveries less effective [24].

Table 3 - Main viral vector used in gene therapy. Adapted from [25, 36, 48].

Virus	Advantages	Disadvantages
Retrovirus	Integration into cellular genome; Broad cell tropism; Prolonged stable expression; Requires cell division for transduction; Relatively high titers (10^6-10^7 pfu/mL)	No targeting; Inefficient transduction; Insertional mutagenesis; Immunogenic problems; Requires cell division for transfection; Potential replication competence
Adenovirus	Extremely high titers (10^{12} pfu/mL); High transduction efficiency *ex vivo* and *in vivo*; Transduces many cell types; Delivers large DNA particles	Remains episomal; Transient expression; Potential replication competence; No targeting; Pre-existing immunity
AAV	Prolonged expression; Transduction does not require cell division; Small genome, no viral genes; Non-pathogenic virus	Low titer production; Potential insertional mutagenesis; Limited insert size: 5kb
Herpes Virus	Large insertional size: 40-50kb; Neuronal tropism; Latency expression; Efficient transduction *in vivo*	Cytotoxic; No targeting; Transient expression; Potential oncogenic response
Lentivirus	Long term gene expression; Infects non-dividing and dividing cells; Relatively high titers (10^6-10^7 pfu/mL)	Generation of replication-competent virus; Potential for tumorigenesis; Difficult manufacture and storage; Safety concerns

1.2.3 Non-viral Vectors

Due to the drawbacks associated with viral vectors, researchers have sought safer alternatives, leading to the development of non-viral vectors for DNA transfer. Non-viral vectors offer several advantages, such as safety, minimal immune response, ease of preparation at low cost and in large quantities. Additionally, they can efficiently transfer diverse and large transgenes and exhibit long-term stability, allowing for extended storage periods. These DNA delivery systems are categorized into physical and chemical [25].

Physical gene delivery systems operate on the principle of utilizing mechanical, ultrasonic, electric, hydrodynamic, or laser-based energy to create temporary weak points in the membrane of the target cell (Table 4). These energy-based techniques cause transient injuries or defects in the membrane, facilitating the diffusion of DNA into the cell [25]. Although conceptually simple yet powerful means for transfecting cells, such methods are expensive and inconvenient for most gene delivery applications [36].

Table 4 - Physical gene delivery systems. Adapted from [25, 32, 36, 49].

	Advantages	**Disadvantages**
Electroporation	Safe; High Efficiency; Reproducible; Low cost; Large size limit	Tissue/cell damage; Invasive; DNA instability
Gene Gun	High level of gene expression; Long-lasting gene expression; Able to reach numerous organs; High efficiency; Safe	Surgery is necessary in order to use for deep tissue; Poor penetration of particles; Tissue/cell damage
Ultrasound	Safe; Non-invasive; Does not need surgery to reach internal organs	Low efficiency; Low reproducibility; Tissue/cell damage
Microinjection	High efficiency; Simple and reproductible; Low cytotoxicity; Large size limit	Time consuming; Inability to transfect large number of cells

In chemical vectors, DNA is delivered into the nucleus using a carrier (Table 5). These vectors have three primary objectives to enhance gene transfer into the cell nucleus. First, they mask the negative charges of DNA, then compress the DNA molecule to reduce its size, and finally protect it from degradation by intracellular nucleases. These aims are achieved by packing DNA through electrostatic interactions between anionic DNA and polycations, encapsulating it or absorbing it [25]. Chemical vectors effectively address various challenges in gene transfer, including extracellular stability, specific cell targeting internalization, endosomal escape, nuclear envelope entry, nucleic release, and genomic integration [32]. Thus, conjugation of pDNA with a carrier, ensures pDNA protection and leads to higher transfection efficiency.

Table 5 – Chemical delivery systems. Adapted from [32, 36, 50]

	Advantages	**Disadvantages**
Cationic Polymers	Suitable for airway gene delivery; Low cytotoxicity; Inexpensive	Aggregates formation; Accumulates in major tissues; Low transfection efficiency *in vivo*
Cation Lipids	Low production cost; Target specificity; Low cytotoxicity	Aggregates formation; Induces inflammatory response; Low transfection efficiency
Inorganic Nanoparticles	Low cytotoxicity; Possibility of functionalization; Efficient transfection	Instability; Toxicity

1.3 Nanotechnology

Nanotechnology involves and refers to the production, development, and application of man-made or engineered particles and molecular structures that measure within the nanometer range, typically ranging from 1 to 100 billionth of a meter. This means that nanomaterials can consist of anywhere from a few hundred to millions of atoms. At this scale, the physical characteristics of chemical elements and larger materials alter drastically due to the increased surface-to-area ratio. The nanoscale changes in physical properties such as colloidal properties, solubility, and catalytic activity are proving to be quite beneficial in various areas of biotechnology. For instance, they are utilized in developing new methods of separation, filtration, pharmaceutical actives, and drug delivery methods. Thus, nanotechnology holds enormous potential for biotechnology applications [51, 52].

1.3.1 Nanoparticles

Nanoparticles (NPs) can be defined as ultra-dispersed solid supramolecular structures with sizes ranging from 10 to 100 nm [53]. They can be manufactured from a range of materials, including metals, metal oxides, polymers, and carbon-based compounds. These tiny particles have special physical and chemical characteristics that make them helpful in a variety of industries, such as electronics, energy, and medicine. The high surface area to volume ratio of nanoparticles is one of their main advantages, due to this, they are extremely reactive and can interact with their environment in ways that larger materials cannot. This characteristic has been used as the foundation for the development of several nanoparticle-based technologies, including drug delivery systems, biosensors, and catalytic converters [52, 54].

1.3.1.1 Types of Nanoparticles

Numerous libraries of nanoparticles have been developed by scientists, and new kinds of particles are constantly being added to this collection. Based on their form, size, and chemical characteristics, NPs are extensively categorized. Each type of NPs can be produced using different techniques, which will determine its characteristics [52, 55].

First described in 1965, liposomes are versatile lipid-based nanoparticles. Described as spherical vesicles with a lipid bilayer membrane and an aqueous interior, lipid NPs have a solid core and matrix containing soluble lipophilic molecules [55–57]. Furthermore, they offer significant benefits in terms of enhancing drug penetration and decreasing systemic administration time through lipophilicity/hydrophilicity and enhanced permeability and retention (EPR) effect [58].

Polymeric nanoparticles (PNPs) are small particles with dimensions ranging from tens to hundreds of nanometers that are made of synthetic or biodegradable polymers. To lessen immunological interactions and intermolecular interactions between the surface chemical groups of PNPs, they are typically coated with non-ionic surfactants. PNPs have been extensively investigated as therapeutic carriers due to their ability to encapsulate hydrophilic or hydrophobic small drug molecules, proteins, and nucleic acid macromolecules. Additionally, they have been used in drug delivery for cervical cancer due to their characteristics of flexible controlled-release, tumour microenvironment (TME) responsive, and improved solubility of insoluble anti-cancer drugs [54–56, 58].

Carbon nanoparticles, including fullerenes and carbon nanotubes (CNTs), have unique properties that make them attractive for biomedical applications such as drug delivery [52, 57]. Fullerenes are globular hollow cages made of carbon atoms with unique electrical properties and high strength, while CNTs are cylindrical graphene sheets with high surface area and excellent electronic and thermal conductivity [54, 59]. Carbon nanocarriers' biocompatibility may be improved by chemical modification of their surface [56].

Metallic particles are made from metal precursors with a size range between 15 and 60 nm [57]. These types of nanoparticles possess unique optoelectrical properties that make them ideal for use in biomedical imaging and therapeutic applications. Moreover, they can be synthesized in a controlled manner to achieve specific size and shape characteristics [54]. Similarly, superparamagnetic nanoparticles, such as those made of iron oxide, have been used in selective magnetic bioseparations, targeted pharmaceutical delivery, and gene transfection. They possess the ability to be attracted to a magnetic field without retaining residual magnetism, allowing for easy handling with the aid of an external magnetic field [52, 56]. The combination of magnetic and metallic nanoparticles presents a promising platform for drug delivery due to their ability to be visualized using magnetic resonance imaging (MRI) and enhanced uptake by the target tissue, resulting in effective treatment [56].

Ceramic nanoparticles, also known as nanoceramics, are inorganic non-metallic solids that are synthesized through heating and cooling processes [60]. They exhibit diverse forms, such as amorphous, polycrystalline, dense, porous, and hollow structures [54]. Furthermore, these nanoparticles possess unique physiochemical properties that lead researchers to explore them as potential materials for delivery systems, which include, facile preparation and functionalization, high transfection efficiency and good biocompatibility and storage stability. Some examples of this type of nanocarriers

include carbon nanotubes, calcium phosphate nanoparticles and silica nanoparticles [51, 61]. Due to these characteristics this type of nanoparticles find utility in the medical field, for bone repair and imaging, and in various industries, contributing to catalysis, photocatalysis, photodegradation of dyes [54, 60].

1.3.2 Calcium Phosphates

Calcium phosphate nanoparticles (CaP-NPs) were first introduced in the 1970s as a non-viral gene delivery system for gene transfection. Since then, they have gained significant recognition as versatile drug delivery systems capable of incorporating imaging probes for cancer diagnosis and bioactive compounds for cancer therapy [62]. These nanoparticles present properties similar to the inorganic mineral found in human bones, making them highly biocompatible and biodegradable materials, which renders them well-suited for applications in orthopedic implants, bone tissue engineering, and nanomedicine drug delivery [63]. The physical and chemical characteristics of CaP-NPs play a pivotal role in their cellular entry and bioactivity. They also, exhibit exceptional mechanical strength, low toxicity, environmentally friendly production methods and, demonstrate a strong affinity for proteins and nucleic acids, ensuring the protection of sensitive biomolecules, and enabling targeted delivery to specific cells [64]. Their rapid degradation and responsiveness to pH variations make them suitable for efficient cellular drug delivery. Moreover, CaP-NPs can be easily modified and functionalized for diagnostic and therapeutic applications [65]. Overall, the unique properties and favourable biological responses of CaP-NPs position them as promising candidates for a wide range of medical applications.

1.3.2.1 CaP-NPs Preparation Methods

Numerous methodologies have been devised to produce CaP-NPs with a wide range of sizes, shapes, and compositions, specifically designed for biological and medical applications in the nanoscale domain. These synthesis methods can be broadly classified as wet-based methods and dry-based methods [66].

The wet-based methods encompass chemical precipitation, sol-gel, hydrothermal, solvothermal, microwave-assisted and sonochemical (Table 6) [67, 68]. One of the key advantages of the wet-based synthesis method is the ability to adjust external parameters to precisely control the morphology and mean size of the resulting CaP powders. However, it is worth noting that the lower temperature utilized in these methods can impact the reaction efficiency and may result in the presence of impurities and reduced crystallinity in the particles [66].

The wet chemical precipitation method is a straightforward and effective technique for producing CaP nanomaterials, such as amorphous CaP and hydroxyapatite. This method involves dissolving precursors in an aqueous medium at low temperatures, eliminating the need for organic solvents and making it an environmentally friendly process. Controlled conditions, such as pH concentration, temperature, and reaction time, are employed to achieve desired biomaterial properties [67]. An advantageous aspect of this approach is its ability to include (bio)organic compounds during synthesis, without risking denaturation of biomolecules like nucleic acids or proteins, as observed in high-temperature or organic solvent-based syntheses [69]. Despite its widespread use and straightforward nature, this method does have limitations, including long reaction times, incomplete reactions, and suboptimal properties for certain applications [67].

The hydrothermal method entails conducting reactions at high temperature and pressure within an autoclave or pressure vessel [66]. This approach results in relatively stoichiometric, highly crystalline, and well-dispersed nanoparticles with controlled morphology and narrow size distribution [70]. However, it is worth noting that the method can be costly and offers limited control over the morphology and size distribution of the nanoparticles [66].

The solvothermal synthesis method is a modified version of the hydrothermal approach that employs organic solvents instead of water. By using organic solvents, higher temperatures and pressures can be achieved, leading to enhanced reactant solubility and faster reaction rates. This versatility allows for the fabrication of a wide range of structured nanomaterials, including coatings on metallic implants. The process involves

mixing starting materials in a solvent, heating the mixture in a sealed container, and subsequently washing and drying the resulting product [67].

The sol-gel method can produce CaP nanomaterials with high purity and controllable morphologies, making it suitable for various biomedical applications, including bone tissue engineering [67]. This preparation method confers advantages, such as molecular-level mixing, resulting in stoichiometric structures with a large surface area. Its simplicity, high versatility, relatively uniform product composition (e.g., Ca:P ratio), and low synthesis temperature making it a favourable option. However, it should be noted that the sol-gel method may generate secondary phases and necessitate the use of expensive starting materials [67, 70].

Microwave-assisted synthesis accelerates chemical reactions by heating the mixture with microwaves. The process includes dissolving soluble materials in a solvent, adjusting the pH value of the mixture, subjecting it to microwave irradiation at a fixed temperature and time, and ultimately isolating the product through centrifugation, cleaning, and drying. This method provides benefits such as shorter synthesis times and enhanced energy efficiency. However, it should be noted that microwave-assisted synthesis may cause some deterioration of the sample constituents and entail higher maintenance costs for industrial-level equipment [67, 71].

Sonochemical methods have proven to be highly beneficial in CaP-NP synthesis, resulting in more uniform products with smaller and spherical particles, higher crystalline fraction, and specific surface area, while minimizing agglomeration [72]. Compared to other synthesis approaches, sonochemical synthesis offers several advantages, including enhanced safety and environmental friendliness as it eliminates the need for toxic solvents. Moreover, this method can be conducted at relatively low temperatures and standard pressure, leading to reduced energy consumption and process costs. Another advantage of sonochemistry lies in its capability to modify the surface properties of materials, such as increasing porosity, improving biocompatibility, and enhancing drug delivery capabilities [67].

Table 6 – Wet methods for the preparation of CaP-NPs. Adapted from [66, 67, 69, 73, 74]

Methods	Morphology	Advantages	Disadvantages
Wet chemical	Diverse	Simple, efficient; Easy control of the reaction system environment	Needs a long reaction time; Difficult to purify composites
Precipitation	Needle-like, spherical and rod-like nanocrystals	Easily synthesized by a low-cost process;	Upscaling can be difficult and requires a continuous process;
Hydrothermal	Needle-like, spherical nanocrystals and nanorods	High crystallinity and purity; The size and morphology can be well controlled	Needs special devices; Time-consuming process and the yield is very low
Solvothermal	Diverse	Short reaction time; Simple operation process	Security risks in the reaction process; Hard to control materials' properties; High energy consumption
Sol-gel	Aggregated nanocrystals	Simple synthesis process; Excellent calcium phosphate crystallization	Needs high sintering temperature and is a time-consuming process; Difficult upscaling; Organic solvents required; Physicochemical properties are uncontrollable; Mixed with impurities
Microwave-assisted	Bowknot, rod, needle-like and flower structures	Short reaction time; Less raw material consumption; Morphology can be well controlled;	Raw materials require full dissolution; Limited application range; High equipment maintenance costs
Sonochemical	Needle-like	Low cost of the process;	Few studies on the preparation of calcium phosphate materials; Hard to industrialize

Dry methods are solvent-free techniques that are suitable for mass production of CaP powders (Table 7) [66, 69]. Among these methods are solid-state synthesis, flame-spray pyrolysis, pulsed laser ablation and mechanochemical techniques [64].

Solid-state synthesis is a relatively simple procedure. In this method, precursors are milled and calcined at very high temperatures, resulting in a well-crystallized structure. However, the powder may exhibit heterogeneity in its phase composition due to limited ion diffusion within the solid phase [66].

Flame-spray pyrolysis stands as a versatile technique for large-scale synthesis of CaP-NP. The process involves injecting a solution or dispersion of precursors into a high-temperature flame, where particle formation occurs. With a wide range of precursor options and flexible reactor system engineering, this method is well-suited to produce nanoparticles with diverse properties, particularly for biomedical applications [69]. This type of synthesis offers scalability in particle formation, morphology, and size, surpassing wet and dry-based synthesis methods. The choice of solvents or liquid precursors directly influences the combustion reaction, providing control over primary particle size and material phase. The local temperature and residence time of particles in the flame play a vital role in determining the crystallinity and nanoscale features of the resulting materials [66]. Although it has proven to be highly effective for synthesizing well-crystalline products in high yields, it can present challenges when attempting to disperse materials in nanoparticulate form due to particle sintering. However, the method's versatility extends beyond CaP, as it is also used to prepare metallic and ceramic nanoparticles through ablation from a solid substrate [69].

Pulsed laser ablation has been utilized for the preparation of CaP-NPs from both synthetic and biological CaP substrates. The method relies on ablating nanoparticles from a solid substrate, showcasing its versatility in synthesizing metallic and ceramic nanoparticles. However, when applied to CaP-NPs, its effectiveness may be somewhat restricted compared to other methods that offer greater control over particle size and composition. Despite the advantage of yielding well-crystalline products in high quantities, one of the challenges with pulsed laser ablation lies in dispersing the material in nanoparticulate form due to particle sintering. Consequently, achieving uniform nanoparticle dispersion can be more difficult with this method, potentially limiting its full applicability for CaP-NPs preparation [69].

The mechanochemical method, also known as mechanical alloying, is another dry approach used to fabricate advanced materials, including nanocrystalline alloys and ceramics. Powder synthesized using this method possesses a well-defined structure due

to the perturbation of surface-bonded species, resulting in acceptable microstructure and reproducibility [66].

Table 7 – Dry-methods for the preparation of CaP-NPs. Adapted from [66, 67, 69, 73]

Methods	Morphology	Advantages	Disadvantages
Solid-state synthesis	Diverse	Easy and low cost; Well-crystallized particles; High yield	Agglomerated particles; Poor redispersability; Application of organic compounds possible only after the synthesis
Flame-spray pyrolysis	Diverse	Good crystallinity; Possibility for scale-up	Particle agglomeration; No incorporation of organic molecules possible; Special equipment necessary
Pulsed laser ablation	Spherical nanostructures	Control over product properties possible by adjustable laser parameters	Tendency for particle agglomeration; high-end laser equipment needed; difficult scale-up
Mechanochemical	Fibrous and spherical nanostructures	Simple and low-cost; No high sintering is needed	Nanocrystals tend to aggregate; needs special devices

1.3.2.2 Types of Calcium Phosphates

The family of CaPs ($CaPO_4$-based) is commonly characterized based on their chemical composition, crystallinity, and morphology. The key distinctions among these CaPs lie in their Ca/P ratio and solubility, with hydroxyapatite (HA) exhibiting the highest Ca/P ratio and displaying the least solubility in a physiological environment. Consequently, the resorption kinetics of CaPs heavily rely on the Ca/P ratio, offering the opportunity to tailor *in vivo* bioresorbability and select the most appropriate phase composition of CaPs for specific applications [75].

Due to their exceptional characteristics, such as biocompatibility, bioactivity, nontoxicity, and osteoconductivity, CaP plays a vital role as bone grafts, bone fillers, and coating materials. Additionally, they can serve as local drug delivery systems to introduce medicines directly into mineralized tissue. CaP can be obtained in different crystalline or amorphous phases, depending on the synthesis conditions, resulting in materials with varying Ca/P molar ratios and distinct physicochemical and biological properties, including solubility, biodegradability, and bioactivity [76].

In total, there are 7 main types of CaP of biomedical interest, amorphous calcium phosphate (ACP), monocalcium phosphate (MCP), dicalcium phosphate (DCP), octacalcium phosphate (OCP), tricalcium phosphate (TCP), hydroxyapatite (HA) and tetracalcium phosphate (TTCP) [76].

Amorphous calcium phosphate (ACP) is a hydrated, transient phase that forms during the precipitation of more stable CaPs in aqueous systems. ACP is typically obtained through wet precipitation in an aqueous medium at low temperatures. Its formation requires specific conditions, such as low or room temperature, high supersaturation, and a pH close to ten. The reaction involves the double decomposition of calcium and phosphate salts in an aqueous or water-alcohol medium, followed by rapid mixing and precipitate filtration. The structure and chemical composition of ACP depends on the pH and composition of the mother solution from which it forms [76].

Monocalcium phosphate (MCP), can be presented in its anhydrous and monohydrate (MCPM) forms. The anhydrous form of MCP is obtained by heating MCPM above 100 ^{0}C. Both MCPM and MCP are not biocompatible due to their highly acidic nature and high solubility [77, 78].

Dicalcium phosphate dihydrate (DCPD), also known as brushite or calcium hydrogen phosphate dihydrate, is a crystalline form of CaP. The DCPD crystals are composed of CaP chains aligned in parallel, with water molecules located between these chains. DCPD is naturally found in dental calculi, urinary stones, and precipitates associated with

chondrocalcinosis. In laboratory conditions, it readily crystallizes from aqueous solutions and remains stable in acidic environments, specifically within a pH range of 4 to 6. It is commonly obtained through wet precipitation methods [76].

Octacalcium phosphate (OCP) is commonly produced under high temperatures and is regarded as an unstable transitional phase in the precipitation of a CaP compound, which exhibits greater thermodynamic stability [77, 79]. One of its key advantages is the stability at neutral pH, making it particularly valuable for medical applications [76].

Tricalcium phosphate (TCP), represented by the general formula $Ca_3(PO_4)_2$, exists in two allotropic forms known as α and β-TCP. Among them, α-TCP presents higher stability temperatures but lower solubility [76]. Despite both α-TCP and β-TCP having a Ca/P ratio of 1.50, they differ in their crystal structures, leading to variations in their thermodynamic behaviour and dissolution rates *in vivo*, α-TCP degrades at a faster rate compared to β-TCP [75]. Similar to HA, an important characteristic of TCP is the ability, to form a strong bond with mineralized tissue, promoting bone formation. Its relatively higher solubility makes it a common component in CaP cements and other bone substitutes [76].

Among all CaPs, HA stands as the most extensively studied material. Its formula, $Ca_{10}(PO_4)_6(OH)_2$, is similar to the biological apatite, which is the primary component of the inorganic part of human mineralized tissues. This likeness makes HA an attractive material, employed either as a standalone bioceramic or as a component in hybrid composites for biomedical engineering applications [76]. In the physiological environment, HA is typically observed in the form of nano-sized rods, measuring 30 to 50 nm in length, 15 to 30 nm in width, and 2 to 10 nm in thickness [75]. HA possesses an ionic character, and its crystalline structure can be described as a hexagonal arrangement of oxygen atoms with metals placed on the tetrahedral and octahedral sites [80]. However, it is important to note that HA is not soluble under *in vivo* conditions [75].

Tetracalcium phosphate (TTCP), unlike other non-apatitic CaPs, cannot be easily synthesized using standard wet methods. It requires higher temperatures when compared to other CaPs and presents an alkaline pH being usually used as an antimicrobial agent [77, 81]. Furthermore, TTCP stands as the sole CaP possessing a higher Ca/P ratio than HA and, similar to HA, it is insoluble [76, 82].

1.3.2.3 Calcium Phosphates in Cancer Environment

CaP has remarkable bioactivity and customizable biodegradability, setting them apart from other biominerals and rendering them highly suitable for drug delivery in nanomedicine applications, as well as in orthopedics, dentistry, and vaccines adjuvants. Their inherent properties, such as pH-dependent solubility, and ease of preparation and functionalization, make them invaluable in various therapeutic areas, including cancer therapy. Biodegradable nanoparticles are particularly favoured in cancer treatment due to their predictable clearance pathways, ensuring their safety for clinical use [63].

Furthermore, the site-specific cellular entry of CaP-NPs plays a pivotal role in the effectiveness and availability of delivered biomolecules. Extensive research has highlighted that crucial factors such as size, charge, morphology, composition, and surface chemistry of CaP-NPs significantly influence the internalization route of nanomedicines. Understanding and optimizing these parameters are essential for enhancing the efficacy and success of nanomedicine-based treatments [63].

1.3.2.3.1 CaP-NP Properties to Overcome Extra and Intracellular Barriers

The cellular entry pathway and ultimate intracellular localization significantly influence crucial factors like the dosage and functionalities of bio-agents. Given the cell's multitude of organelles, precise delivery of the therapeutic payload to a specific site becomes vital to elicit the desired effect. Understanding the mechanisms through which cells transport their components to distinct cellular compartments can offer valuable insights, thereby enhancing drug design and leading to more effective tumour management strategies [63].

Nanoparticle size and morphology significantly influence their interactions with cell membranes, intracellular trafficking, pharmacokinetics, extravasation, and clearance mechanisms. Specific cell membrane receptor binding and internalization are modulated by these factors. When considering CaP in cancer therapy, a straightforward preparation method involves synthesizing them in the presence of nucleic acids such as DNA, siRNA, and oligonucleotides, resulting in larger particles (100 to 200 nm). However, these larger nanoparticles tend to have a brief blood circulation time due to rapid accumulation in the reticuloendothelial system (RES), while ultrasmall nanoparticles smaller than 8 to 10 nm are rapidly cleared from the bloodstream via renal processes [63, 83].

To achieve consistent particle size and morphology in CaP nanoparticle synthesis, careful selection of precursors and their concentrations is essential. After the initial nucleation burst, particle aggregation becomes a challenge, driven by van der Waal's and secondary

surface interactions, especially in the nano-sized range where nanoparticles exhibit heightened intrinsic surface reactivity. Striking the optimal balance, CaP-NP synthesis should be finely tuned to produce sizes within the range of 10 to 80 nm, aligning with recommendations for other nanoparticle types. This optimization facilitates longer blood circulation time and improved uptake by tumours, enhancing their effectiveness in cancer therapy [63].

Recent studies *in vivo* cancer therapy utilizing CaP have predominantly employed spherical CaP-NPs or shells to deliver therapeutic agents to cancer tissues. This preference is primarily due to the mild mineralization conditions utilized in CaP preparation, which tend to yield thermodynamically stable spherical and round morphologies. On the other hand, rod-shaped morphologies have been synthesized using relatively higher temperature methods. However, for therapeutic delivery applications, spherical nanoparticles are generally favoured as they offer the highest specific surface area for loading drugs or nucleic acid molecules [63].

In addition to spherical nanoparticles, other CaP morphologies, such as nano-clusters and porous structures, have been explored as potential high-loading capacity candidates for cancer therapy applications. However, their relatively larger size and the involvement of multiple synthesis steps are perceived as significant drawbacks that hinder their potential application in clinical trials. Consequently, spherical CaP-NPs remain the more promising and preferred option for efficient and effective drug delivery in cancer therapy research [63].

The biodegradation of drug carriers before reaching the target site raises concerns about patient safety, especially with biodegradable polymeric nanoparticles. These nanoparticles can potentially alter drug activity and interact adversely with tissues during circulation, due to the production of acidic or degradation by-products [77]. However, CaP solubility is pH-dependent, remaining stable at the human blood pH of 7.4 and in more alkaline environments [67]. Nevertheless, it easily dissolves in low pH environments, such as within endosomes/lysosomes or at tumour sites. In these low pH environments, CaP-NPs dissolve and disassemble, releasing their cargo at the tumour site or within endosomes. This release creates high osmotic pressure, leading to endosome expansion and eventual rupture, which, in turn, releases the cargo, along with Ca^{2+} and PO_4^{3-} ions, into the cytoplasm. It is important to notice that these ions are already present in relatively high concentrations (1 to 5 mM) in the bloodstream, reducing the risk of unwanted side effects caused by these degradation products. This mechanism highlights the potential safety and efficacy of CaP-NPs as drug carriers, as

their biodegradation is carefully regulated by the surrounding environment, ensuring effective drug delivery to the target site while minimizing adverse effects [67, 77].

The biodegradability of CaP-NPs has been demonstrated in studies involving HeLa cells (human epithelial cervical cancer cells). These nanoparticles, measuring 120 nm in diameter, undergo rapid endocytosis by the cells and swiftly dissolve within lysosomes. Moreover, during this process, calcium ions are actively secreted out of the cell. These findings unequivocally confirm the biodegradable nature of CaP-NPs, highlighting their potential as a safe and effective option for various biomedical applications [67].

Another characteristic of CaPs is their resistance to enzymatic degradation in the physiological environment, setting them apart from organic or polymeric nanoparticles. This feature, combined with their limited susceptibility as microbial substrates, contributes to their good storage stability [77].

1.3.2.3.2 CaP-NPs Cell Internalization

The cell membrane, composed of a flexible lipid bilayer, serves as a crucial barrier, separating the intracellular environment from the external surroundings. It plays a vital role in the internalization of therapeutic molecules, including nucleic acids, proteins, and drugs. However, due to their large sizes and hydrophobic nature, most cancer therapeutic agents face challenges in crossing the cell membrane easily and alone. Therefore, the use of nanoscale carriers becomes essential to facilitate the efficient intracellular delivery of these therapeutic agents. These carriers enable safe and effective transport of therapeutic molecules into the cells, ensuring enhanced efficacy and precision in cancer treatments [63].

The uptake pathways of synthetic nanoparticles can generally be categorized into two main groups: endocytic uptake pathway and non-endocytic delivery. Endocytosis involves the vesicular uptake of nanoparticles through the invagination and pinching of a part of the cell membrane. Various subgroups of endocytic routes exist, including phagocytosis, macropinocytosis, clathrin-mediated endocytosis, caveolae-mediated endocytosis, and nonclathrin- and noncaveolae-mediated endocytosis [63, 84].

The clathrin mechanism is a multi-step endocytosis process, activated by the binding of ligands on the surface of nanoparticles to specific receptors on the cell membrane. Caveolae endocytosis, on the other hand, involves the small invagination of the cell membrane to internalize the nanoparticles. In contrast, pinocytosis occurs through hydrophobic or electrostatic interactions of nanoparticles with the plasma membrane, following a mechanism similar to the uptake of fluid-phases [63]. Phagocytosis starts with the process of opsonization of the nanoparticles, which are then recognized and

attached to phagocytes which leads to the formation of cell surface extensions and subsequent engulfing and internalization of the nanoparticles. In clathrin- and caveolae independent endocytosis the internalization occurs in cells devoid of both clathrin and caveolae, thus requiring a specific lipid composition [85].

The efficacy of cancer therapeutics using nanoparticles is closely tied to their uptake mechanisms and subsequent biological responses in targeted cells. The exact endocytosis mechanisms of CaP nanoparticles depend on factors such as their surface coating molecules, size, morphology, and the type of targeted cells. For instance, a study using HeLa cells reported the clathrin pathway as the major endocytosis mechanism for 140 nm CaP nanoparticles coated with a co-polymer of PEG and poly-(benzoxaborole). Overall, the literature suggests that the endocytosis mechanism of CaP nanoparticles is contingent on the type of cancer cells and the physicochemical properties of the nanoparticles, including their size, coating molecules, and morphology. Understanding and tailoring these factors are critical for optimizing the therapeutic efficacy of CaP nanoparticles in cancer treatments [63].

The internalization through a vesicular approach has been identified as the primary mechanism for cellular uptake of CaP nanoparticles in various cancer therapeutic studies [63]. The pathway leads to the encapsulation of NPs within vesicles called endosomes. Subsequently, the endosome fuses with a lysosome, creating an endolysosome with a lower pH around the CaP-NPs, causing their degradation. This degradation process releases a high concentration of calcium and phosphate ions, resulting in water influx by osmosis, leading to lysosome rupture. The released therapeutic molecules enter the cytosol, aided by active transport pumping out excess calcium. The therapeutic molecules are now free to move within the cytoplasm through diffusion, reaching their designated target locations. In the context of delivering DNA molecules, they must transfer into the nucleus through diffusion or dissociation via nuclear pores. Once in the nucleus, the DNA molecules are integrated into replicating strands where they are needed. This intracellular delivery process enables efficient and targeted release of therapeutic agents, including DNA, ensuring their efficacy [86].

1.3.2.3.3 Targeted Delivery of CaP-NPs

The remarkable advancement in CaP-based nanoparticle systems lies in their ability to achieve targeted and localized delivery. This breakthrough ensures that a minimum systemic dosage can effectively produce a maximum therapeutic or bioimaging agent precisely at the desired site, while sparing healthy cells and preserving

therapeutic efficacy. The use of surface markers expressed uniquely on tumour cells offers an ideal approach for targeted drug delivery, by specifically targeting these surface markers, nanoparticles can directly reach and interact with tumour cells, enhancing drug delivery precision, while minimizing off-target effects [87]. In contrast, without a specific cell target, nanoparticles rely on passive diffusion and/or the leaky vasculature of tumours, the EPR effect, to reach the site of interest. However, this passive approach is not always effective and may lead to premature degradation or elimination from circulation, limiting their overall effectiveness [87].

The choice of surface functionalization for CaP nanoparticles depends on the type of targeted tumours and the treatment approaches utilized. Typically, surface functionalization leads to an increase in the hydrodynamic size of CaP nanoparticles due to the addition of large molecules to their surface. Larger hydrodynamic sizes are associated with shorter blood circulation time and reduced uptake by tumours, as mentioned earlier. However, the incorporation of PEG onto the surface of CaP nanoparticles can help extend their blood circulation time by creating steric hindrance and minimizing protein adsorption [63].

Achieving targeted delivery of CaP nanoparticles to tumours is crucial for enhancing therapeutic efficacy and minimizing off-target effects. Effective methods to improve specific targeting involve covalent or non-covalent binding of peptides or antibodies to the surface of CaP nanoparticles. The selection of targeting molecules to be conjugated to CaP nanoparticles depends on the type of cancer cells and the receptors present on their membranes [63]. Various targeting ligands, such as proteins (antibodies or antibody fragments), peptides (arginine-glycine-aspartic acid or RGD), vitamins (folic acid), nucleic acids (aptamers), and glycoproteins (transferrin), are extensively used as nanocarrier surface modifiers for the development of cancer-targeted delivery systems. By utilizing these diverse targeting ligands, researchers are advancing the development of highly effective and tumour-specific nanocarriers for cancer therapy [88].

Folate, a water-soluble form of vitamin B9, plays a vital role in facilitating rapid cell division and growth, particularly during embryonic development in humans. Notably, folate receptors are overexpressed in epithelial tumours, such as cervical, ovarian, endometrial, brain, head, neck, renal, colorectal and breast tumours. Due to its high binding affinity for these receptors, $K_d = 10^{-9}$ M, folate has become a widely utilized targeting moiety for imaging and therapeutic agents in tumour treatments [89, 90]. When conjugated to CaP nanoparticles, folic acid, being a small molecule, does not significantly increase their hydrodynamic size. As a result, folic acid proves to be a

suitable targeting molecule, offering the potential for specific delivery of therapeutic agents to tumours using CaP nanoparticles [63].

Folic acid functionalized nanoparticles are known to be internalized via clathrin/caveolae independent endocytic pathway. Folate binds to its receptor, facilitating a non-destructive entry into the cytoplasm. Nanocarriers internalized through folate receptor-mediated endocytosis also escape trafficking into lysosomes and are frequently retained in endocytic compartments or released directly into the cytoplasm [85]. Rout *et al.* reported the functionalization of magnetic calcium phosphate nanoparticles with folic acid and the results showed targeting activity towards cancer cells, with optimal drug delivery and consequent cell death [91].

This targeted approach holds promise for enhancing the effectiveness and precision of delivering therapeutic molecules to tumour sites, while minimizing the impact on healthy tissues [63].

Chapter 2 – Aim of the Thesis

Cervical cancer, primarily resulting from persistent infection with high-risk strains of HPV, ranks as the fourth most common cancer in women, presenting a significant and pressing global health challenge. The disruption of E6 and E7 oncoproteins promotes the invasion proliferation and survival of cancer cells, and leads to the inactivation of p53 and pRb, respectively. Presently, there are no targeted treatments for this disease, underscoring the critical need to devise novel strategies. Thus, utilizing a targeted carrier to deliver plasmid DNA, that could restore the p53 protein level in cancer cells, presents as a promising treatment.

The global aim of this study is to formulate and characterize functional calcium phosphate nanoparticles to deliver plasmid DNA encoding p53 to cervical cancer cells.

In this way, the current research involves the synthesis of calcium phosphate nanoparticles through co-precipitation method, enabling the encapsulation of pDNA and facilitating targeted delivery by incorporating folic acid. For that, the formulation process will be optimized to ensure favourable attributes, including size, charge, pDNA encapsulation efficiency and folic acid loading efficiency. Following the optimization of the various physical and chemical parameters of CaP-NPs, the most promising formulations will be chosen for further investigation of their performance in *in vitro* experiments. These assays will be conducted using two distinct cell lines, human fibroblasts as non-cancerous cell line and HeLa cells as HPV positive cervical cancer cell line, evaluating aspects such as cell viability, transfection efficacy and p53 expression.

Chapter 3 – Materials and Methods

3.1 Materials

For the nanoparticle preparation, sodium citrate tribasic dehydrate ($C_6H_5Na_3O_7 \cdot 2H_2O$, ≥ 99.0 %) from Sigma-Aldrich (St. Louis, EUA), calcium chloride ($CaCl_2$, ≥ 93.0 %) from Honeywell Fluka™ (Germany) and sodium phosphate dibasic anhydrous (Na_2HPO_4) from CARLO ERBA (Cornaredo, Italy) were used. Folic acid ($C_{19}H_{19}N_7O_6$, ≥ 97 %) from Sigma-Aldrich (St. Louis, EUA) was used. For the bacterial cultures, tryptone and yeast extract were obtained from Bioakar Diagnostics and Luria-Bertani (LB) medium in PanReac. Agar and kanamycin were purchased from Thermo Fisher Scientific (Waltham, USA). For the electrophoresis, GreenSafe reagent (GreenSafe Premium) was obtained from NZYTech (Lisbon, Portugal) and agarose was acquired from Hoefer (San Francisco, USA). DMEM/F12 cell culture media was obtained from Gibco, Thermo Fisher Scientific (Waltham, MA, USA). Sodium bicarbonate was obtained from MP Biomedicals (Santa Ana, USA).

All solutions were freshly prepared using ultra-pure grade water, purified with a Milli-Q system from Millipor (Billerica, MA, USA).

3.2 Methods

3.2.1 Plasmid DNA Production

The p53 tumour suppressor gene was inserted into the pMC.CMV-MCS-EF1-GFP-SV40Poly A vector, which includes an antibiotic resistance gene for kanamycin. Subsequently, the pDNA containing the p53 gene was amplified in ZYCY10P3S2T *Escherichia coli* host strain. Initially, the *E. coli* strain was inoculated on Luria-Bertani (LB) agar petri dishes containing 50 µg/mL of kanamycin antibiotic and incubated overnight at 37 ºC to formulate colonies. This solid medium enabled cell recovery from cryopreservation and adaptation to nutrients through direct contact. Following the overnight incubation, isolated colonies were extracted and inoculated into a 250 mL Erlenmeyer flask containing 62.5 mL of Terrific Broth (TB), a pre-fermentation medium. TB medium is composed of 24 g/mL yeast extract, 20 g/L tryptone, 4 mL/L glycerol, 0.017 M KH_2PO_4 and 0.071 M K_2HPO_4, later supplemented with 50 µg/mL of kanamycin. The Erlenmeyer was then placed in the orbital shaker at 42 ºC and 250 rpm, until the optic density at 600 nm ($OD_{600\ nm}$) reached 2.6. Upon reaching the desired value, a

certain culture volume was transferred to a 1 L Erlenmeyer containing 250 mL of TB, to start the fermentation with an $OD_{600\ nm}$ value of 0.2. The fermentation Erlenmeyer was then placed in the orbital shaker under previous conditions, until it reached an $OD_{600\ nm}$ of 5. To harvest the cells, the fermentation solution was divided into 50 mL falcon tubes and centrifuged at 3900 rpm for 10 min at 4 ºC, the resulting pellets were stored at - 20 ºC.

3.2.2 Plasmid DNA Purification

Following the fermentation process, pDNA extraction and purification were performed using the NZYMaxiprep kit (NZYTech, Portugal). The frozen pellet obtained from 125 mL of fermentation was thawed. 10 mL of P1 solution (50 mM Tris, 10 mM EDTA, 100 µg/mL of RNase, pH 8) was added to the falcon tube and vortexed. Subsequently, the content was transferred to a lysis tube, and 10 mL of P2 solution (200 mM NaOH, 1 % SDS) was added. The centrifuge tube was gently inverted and incubated for 5 min at room temperature. To stop the lysis process, 10 mL of P3 solution (3 M potassium acetate, pH 5.5) was added to the centrifuge tube, and the homogenization was repeated. The tube was then placed on ice for 20 min. Afterwards, the tubes were centrifuged twice at 20 000 g for 30 min at 4 ºC, and the supernatant was carefully transferred to a clean lysis tube between centrifugations. A silica-based anion exchange column was employed to selectively bind the pDNA. To equilibrate the columns the 10 mL of QBT (750 mM NaCl, 50 mM MOPS, 0.15 % Triton-X 100, 15 % isopropanol, pH 7) was added. The supernatants were added to the column. Next, the columns were washed twice with 30 mL of QC (750 mM NaCl, 50 mM MOPS, 15 % isopropanol, pH 7) to eliminate unwanted impurities. Subsequently, a clean lysis tube was placed on ice, and the column was positioned on top. The QF (1.25 mM, 50 mM Tris, 15 % isopropanol, pH 8.5) solution was then used to elute the pDNA from the column. After the elution step, 10,5 mL of isopropanol was added to the tube and the solution was gently homogenized and incubated for 20 min on ice. The solution was centrifuged at 16 000 g for 30 min at 4 ºC. The supernatant was discarded, and the pellet was resuspended in 1 mL of Tris-EDTA buffer solution. The column was regenerated with an adequate solution (3 M NaCl, 0.15 % Triton X-100), thoroughly washed and stored in ethanol 20 % at 4 ºC for future use. Finally, the nanophotometer equipment was used to measure the final concentration of the pDNA sample at 260 nm, which was subsequently stored at - 80 ºC.

3.2.3 Agarose Gel Electrophoresis

Throughout this work, the agarose gel electrophoresis was prepared at 0.8 % (w/v), in 1x Tris-Acetate-EDTA (TAE) buffer (40 mM Tris, 20 mM acetic acid, 1 mM EDTA, pH 8) and stained with 0.6 µL of Green Safe (NZYTech, Portugal). An amount of 18 µL of sample with 2 µL of loading buffer was added to each well. The loading buffer is composed of water, glycerol, and bromophenol blue. The electrophoresis run was carried out for 40 min at 110 mV and the gel was analysed through Uvitec Fire-Reader system (UVITEC, United Kingdom).

3.2.4 Calcium Phosphate Nanoparticle Formulation

The preparation of the CaP- NPs was done according to Di Mauro and co-authors [92]. Firstly, an aqueous solution of calcium chloride hexahydrate (100 mM) and sodium citrate tribasic dihydrate (400 mM) and an aqueous solution of sodium phosphate dibasic anhydrous (120 mM) were prepared. For the nanoparticle formulation the calcium and citrate solution was mixed with the phosphate solution and the pH was adjusted with a sodium hydroxide solution (0.1 M). The resulting solution was incubated at 37 ºC for 5 min, and rapidly cooled in ice. To remove unreacted reagents, nanoparticles were washed 3 times by centrifugation, 3000 rpm for 5 min at 4 ºC, with ultrapure water.

For the formulation of CaP-NPs with pDNA (CaP-NP/pDNA), the previous protocol was followed. After the last centrifugation, the supernatant was discarded, and the pellet resuspended in PBS (Phosphate Buffered Solution) without calcium and magnesium. Subsequently, pDNA was added to the CaP-NPs at a concentration of 20 µg/mL, and the mixture was left to incubate overnight at 4 ºC. Following the incubation process, the nanoparticles were repeatedly washed through centrifugation, as described earlier.

For the inclusion of folic acid in the CaP-NP/pDNA (CaP-NP/pDNA/FA) two approaches were performed. In the first one, folic acid was added to the calcium and citrate solution and the rest of the protocol remained unchanged. In the second approach, like the pDNA incorporation, folic acid was added, at the same time as pDNA, to the CaP-NPs after the last centrifugation and incubated overnight at 4 ºC. Folic acid was added at a concentration of 0.01 mg/mL [93]. Following the incubation process, the nanoparticles were repeatedly washed through centrifugation.

An overview of the preparation methods is described in Table 8.

Table 8 – Overall view of preparation conditions for each formulation.

<table>
<tr><th>Formulation</th><th>Precursor Solutions</th><th>Washing Parameters</th><th>pDNA Addition</th><th>Folic Acid Addition</th></tr>
<tr><td>CaP-NP</td><td rowspan="4">• 100 mM solution of calcium chloride hexahydrate
• 400 mM solution of sodium citrate tribasic dihydrate
• 120 mM solution of sodium phosphate dibasic anhydrous</td><td rowspan="4">3 Washes at 3000 rpm for 5 min</td><td>-</td><td>-</td></tr>
<tr><td>CaP-NP/pDNA</td><td rowspan="3">Overnight adsorption at 4 ºC</td><td>-</td></tr>
<tr><td>CaP-NP/pDNA/FACa</td><td>Precursor calcium solution</td></tr>
<tr><td>CaP-NP/pDNA/FAAd</td><td>Overnight adsorption at 4 ºC</td></tr>
</table>

3.2.5 Physical and Chemical Characterization of The Delivery Systems

3.2.5.1 CaP-NPs Size and Charge

The size, PdI and zeta potential measurements were obtained by Dynamic Light Scattering (DLS) at 25 ºC using a Zetasizer Nano ZS equipment (Malvern Instruments, UK) and the Malvern Zetasizer software v6.36. The nanoparticle solution was mixed with ultra-pure water in a final volume of 1 mL and placed in a folded capillary zeta cell. All parameters were measured three times from three independent samples.

3.2.5.2 Fourier Transform Infrared Spectroscopy

To evaluate the chemical composition of the nanoparticles and the presence of folic acid, fourier transform infrared spectroscopy (FTIR) was performed. Each formulation was freeze-dried at -20 ºC and lyophilized overnight using a ScanVac Coolsafe freeze dryer (Labogene, DK). The spectra of each formulation were acquired using a Nicolet iD10 FTIR spectrophotometer (Thermo Scientific, Waltham, USA) with an average of 120 scans, a spectral resolution of 32 cm^{-1} and a spectral width range of 4000-400 cm^{-1}.

3.2.6 Encapsulation Efficiency

To determine the encapsulation efficiency of pDNA and folic acid in the CaP-NPs a straightforward protocol was used. After the overnight incubation, the CaP-NP/pDNA, CaP-NP/FA (CaP-NPs with folic acid) and CaP-NP/pDNA/FA were washed three times with ultrapure water, and each supernatant was recovered and quantified using xMark™ Microplate Absorbance Spectrophotometer (Bio-Rad) at a wavelength of 260 nm for pDNA and 280 nm for folic acid. To perform the quantification, calibration curves were performed using standard concentrations of pDNA and folic acid dissolved in PBS without calcium and magnesium were generated. The measurements were conducted with replicates (n=3) and from various samples to ensure accuracy and reliability.

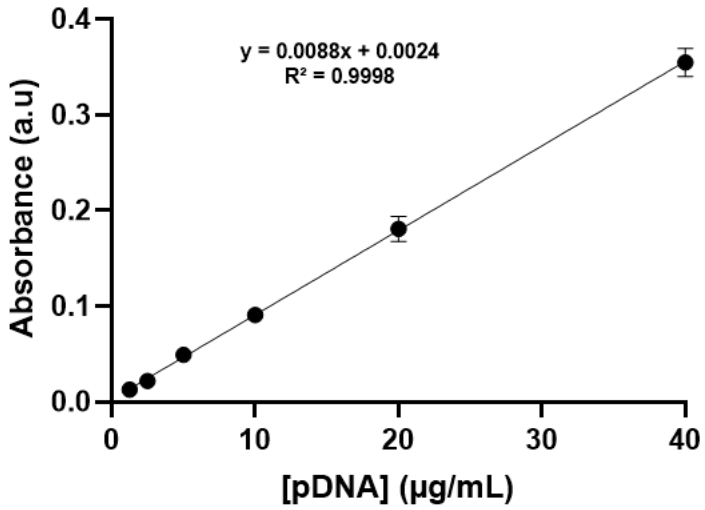

Figure 5 – Graphical representation of the pDNA calibration curve (1.25-40 µg/mL). Data is presented as mean ± SD for three independent experiments (n=3).

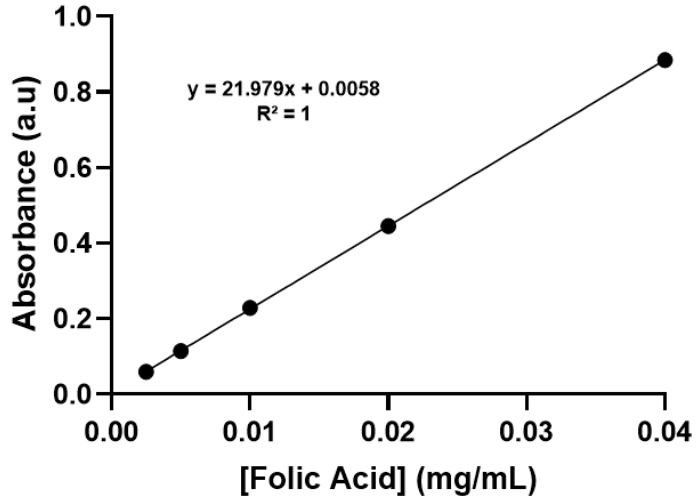

Figure 6 - Graphical representation of the Folic Acid calibration curve (0.0025-0.04 mg/mL). Data is presented as mean ± SD for three independent experiments (n=3).

3.2.7 Release Assay

For the determination of released pDNA, the CaP-NP/pDNA were suspended in 1 mL of PBS, without calcium and magnesium, and incubated at 37 ºC to mimic the physiological conditions. Samples were taken at several time points, 30 min, 1, 2, 3, 4, 5 and 6 h, and later the pDNA concentration was measured in xMark™ Microplate Absorbance Spectrophotometer (Bio-Rad, USA) at 260 nm. For the quantification, the previously mentioned calibration curve was used. For a qualitative analysis, an electrophoresis of 0.8 % agarose gel was carried out. A control was done, with CaP-NPs in PBS without calcium and magnesium.

3.2.8 Cell culture Experiments

The *in vitro* experiments were performed in two different cell lines. HeLa cells (HPV-18 positive from cervical adenocarcinoma) and human fibroblast cells were cultured in Dulbecco's Modified Eagle's Medium/ Ham's F-12 nutrient mixture (DMEM-F12), supplemented with 10 % (v/v) of fetal bovine serum (FBS) and a mixture of penicillin (100 mg/mL) and streptomycin (100 mg/mL). Cells were incubated at 37 ºC in a humidified atmosphere containing 5 % CO_2. Cells were seeded in a complete medium and 24 h before transfections experiments this medium was replaced with medium without supplements to promote transfection.

3.2.8.1 Cell Viability Assay

To evaluate the impact of nanoparticles on cell viability, a resazurin assay was employed. This method measures cellular metabolic activity by evaluating the reduction of the non-fluorescent dye resazurin to the strongly fluorescent dye resorufin via mitochondrial reductase.

HeLa cells were seeded with a cell density of 5000 cells per well and fibroblasts were seeded with a cell density of 10 000 cells per well, in 96-well plates. After 24 h the medium was discarded and replaced with non-supplemented medium. The cells were transfected with different concentrations of CaP-NP, CaP-NP/pDNA and Cap-NP/pDNA/FA. 24, 48 and 72 h after transfection, the culture medium was discarded and 100 µL of fresh complete medium and 20 µL of resazurin 0.1 % (w/w) were added to each well. Cells were incubated in the dark over 4 h at 37 ºC in a humified atmosphere containing 5 % CO_2. 100 µL of the mixture was transferred to well in an opaque plate, where the fluorescence was read. The measurements were performed using a plate reader spectrofluorometer (Spectramax Gemini XS, Molecular Devices), with a fluorescence excitation at 544 nm and emission at 590 nm. Two controls were done, a negative control

with non-transfected cells and a positive control, where ethanol 70 % was added to promote cellular death.

3.2.8.2 Internalization Assay – Confocal Microscopy

To assess nanoparticle internalization, the CaP-NPs, CaP-NP/pDNA and CaP-NP/pDNA/FA were marked with fluorescein isothiocyanate (FITC). This compound was added during the nanoparticle formulation, specifically in the calcium and citrate solution at a concentration of 20 μg/mL. Hela cells were seeded with a cell density of 30 000 cells per well and fibroblasts were seeded with a cell density of 60 000 cells per well, in lamellas previously inserted and sterilized into 24-well plates. After 24 h, the medium was discarded and replaced with non-supplemented medium. Cells were transfected with different concentrations of CaP-NP, CaP-NP/pDNA and Cap-NP/pDNA/FA. After 30 min and 2 h, the medium was discarded and 500 μL PBS without calcium and magnesium was used to wash each well. Afterwards, 300 μL of a fixation solution (PFA 4 %) was added and incubated 10 min at room temperature, then the solution was discarded and 500 μL PBS without calcium and magnesium was used to wash each well twice. Finally, the respective plates were stored at 4 ºC with 1.5 mL PBS without calcium and magnesium in each well.

The microscopy pictures were acquired by the confocal microscopy system LSM 710 (Carl Zeiss SMT, Germany) with the Zeiss Zen software.

3.2.8.3 RNA Extraction

The RNA extraction was conducted in two different cell lines. Hela cells were seeded with a cell density of 55 000 cells per well and fibroblasts were seeded with a cell density of 110 000 cells per well, in 12-well plates. After 24 h, the medium was discarded and replaced with non-supplemented medium. Cells were transfected with CaP-NP/pDNA and Cap-NP/pDNA/FA. 24 h after transfection, the medium was discarded, and each well was washed with PBS without calcium and magnesium. The cell lysis was carried out through the addition of 100 μL TripleXtractor (GRiSP, Porto, Portugal) to each well. After that, samples were incubated for 5 min at room temperature and freeze-dried at – 80 ºC. Later, 50 μL of chloroform was added to each sample, to separate the different biomolecules, and a 10 min incubation was carried out at room temperature. The samples were centrifuged at 12 000 g for 15 min at 4 ºC, in which we carefully recovered the aqueous phase where the RNA was present. The RNA precipitation was performed using 125 μL of cold isopropanol and samples were gently homogenized. An incubation of 10 min in ice was carried out and samples were centrifuged at 12 000 g for 15 min at 4 ºC. The pellet was recovered and resuspended in 125 μL 75 % ethanol, to eliminate the

organic compounds. Another centrifugation was conducted at 12 000 g for 5 min at 4 ºC, and the pellet was resuspended in diethylpyrocarbonate (DEPC) water. To confirm the RNA extraction, a 1 % agarose gel electrophoresis was carried out and the sample quantification was done in a NanoPhotometer.

3.2.8.4 cDNA Synthesis

The cDNA synthesis was done with Xpert cDNA Synthesis kit (GRiSP Research Solutions, Portugal). A mixture of 1 µg of total RNA, 1 µL of random primers, 1 µL of deoxynucleotide (dNTP), 4 µL of reaction buffer, 1 µL of Xpert RTase and RNase free water until the final volume of 20 µL was prepared. The mix was gently homogenized, and the samples were incubated at 25 ºC for 10 min. Using the thermocycler, three cycles were performed, the first for 10 min at 25 ºC, the second for 50 min at 50 ºC and the last for 5 min at 85 ºC.

3.2.8.5 Reverse Transcription-Polymerase Chain Reaction (RT-PCR)

Qualitative analysis of p53 transcripts levels was evaluated by Reverse Transcription-Polymerase chain reaction (RT-PCR). For the PCR experiment, a mixture of 0.40 µL of forward primer, 0.40 µL primer reverse, 1 µL of the cDNA sample synthetized previously, 6.25 µL of GRS Taq DNA polymerase and 4.75 µL of RNase free water was used. Samples were then put into the T110™ Thermal Cycler (Bio-Rad, USA), with the following settings, 95 ºC for 5 min, 35 cycles of 30 s at 95 ºC, 30 s at 55.3 ºC and 1 min at 72 ºC, finally 10 min at 72 ºC. The results were analysed through a 1 % agarose gel electrophoresis.

3.2.8.6 Statistical Analysis

Each assay was performed at least three times. Data are expressed as a mean ± standard error (S.D.). The statistical analysis performed was a one-way analysis of variance (ANOVA). Data analysis was performed in GraphPad Prism 8 Software. A p-value below 0.05 was considered statistically significant. Additionally, significance was determined as ****p-value <0.001, ***p-value < 0.001, **p-value < 0.01 and *p-value < 0.05.

Chapter 4 – Results and Discussion

4.1 Development of Calcium Phosphate Nanoparticles

CaP-NPs have been used as drug delivery systems with various purposes. Depending on the preparation method CaP-NPs can present different sizes and charges. In a study made by Esposti *et al.*, the precipitation method yielded CaP-NPs with sizes ranging from 60 to 140 nm, displaying a negatively charged surface [68]. This delivery platform has the capability to be combined with diverse nucleic acids. For instance, Roy *et al.* successfully introduced plasmid DNA to CaP-NPs through addition of pDNA in precursor solutions, resulting in particles of 80 nm [94]. Another investigation made by Khan *et al.* generated CaP-NP sized around 100 nm, and with the introduction of pDNA in a calcium precursor solution, the mean size increased to approximately 190 nm [95].

The present study focuses on the production of CaP-NPs using a straightforward protocol, with a subsequent evaluation of the impact of the nanoparticle washing step on size, polydispersity index (PdI), and surface charge. Briefly, two precursor solution, one containing calcium and citrate and another containing phosphate, were mixed and sodium hydroxide was used to achieve a pH of approximately 9. Then a washing step was performed, to eliminate residual agents, and in this particular case to remove citrate, which is used as a stabilizing agent and regulator of crystal growth, only necessary during the formulation step.

Thus, to optimize the preparation method, the formulation process was kept constant, while centrifugation parameters were manipulated. Initially, an approach previously described in literature was considered, consisting in three washes at 3000 rpm for 5 min [92]. Alternatively, three washes at higher centrifugation speed with different times (4500 rpm for 5 min and 4500 rpm for 10 min) was also evaluated, this centrifugation rate had been previously described in literature [68]. Furthermore, several other approaches were investigated, one wash at 4500 rpm for 10 min, six washes centrifugation at 4500 rpm for 5 min, and six washes at 4500 rpm for 10 min.

Cellular internalization is influenced by several parameters, but the most important are size and charge of delivery systems. Existing literature highlights an optimal size of approximately 100 nm, acknowledging that nanoparticles must exceed 10 nm to evade renal clearance while remaining under 200 nm to evade the reticuloendothelial system (RES). This size range also promotes effective accumulation and retention in tumours via the EPR effect [83, 96]. Charge constitutes another determinant for cellular

internalization. Nanoparticles presenting a zeta potential of around + 30 or - 30 mV are deemed stable in aqueous dispersion due to the surface charge's preventive role against particle aggregation [69]. Moreover, cationic delivery systems exhibit a heightened binding affinity to the negatively charged membranes of target cells compared to their negatively charged or neutral counterparts. However, it is worth noting that cationic systems tend to exhibit higher cytotoxicity compared to anionic counterparts, since cationic systems interact more with the cell membrane leading to membrane disruption [97].

Some studies indicate that negatively charged delivery systems exhibit a lower rate of endocytosis and use the clathrin-mediated endocytosis pathway to a lesser extent [98]. In a study by Sokolova *et al.*, the uptake mechanism of anionic and cationic CaP-NPs in HeLa cells was examined, revealing that these nanoparticles do not inherently induce cytotoxicity. Additionally, cellular uptake is not affected with increased nanoparticle concentration [99].

Thus, the size, PdI and chemical composition of all CaP-NPs, obtained exploring different washing parameters are summarized in Table 9, Figure 7 and 8.

Table 9 – Size and Polydispersity index for CaP-NPs systems obtained with different washing conditions. The values represent the mean ± SD of three independent assays (n=3).

	Size (nm)	**PdI**
1 Wash (4500 rpm; 10 min)	128.373 ± 27.768	0.463 ± 0.037
3 Washes (3000 rpm; 5 min)	76.338 ± 34.081	0.403 ± 0.091
3 Washes (4500 rpm; 5 min)	193.700 ± 46.041	0.553 ± 0.078
3 Washes (4500 rpm; 10 min)	218.967 ± 60.075	0.605 ± 0.093
6 Washes (4500 rpm; 5 min)	333.967 ± 62.434	0.688 ± 0.400
6 Washes (4500 rpm; 10 min)	332.733 ± 202.879	0.564 ± 0.159

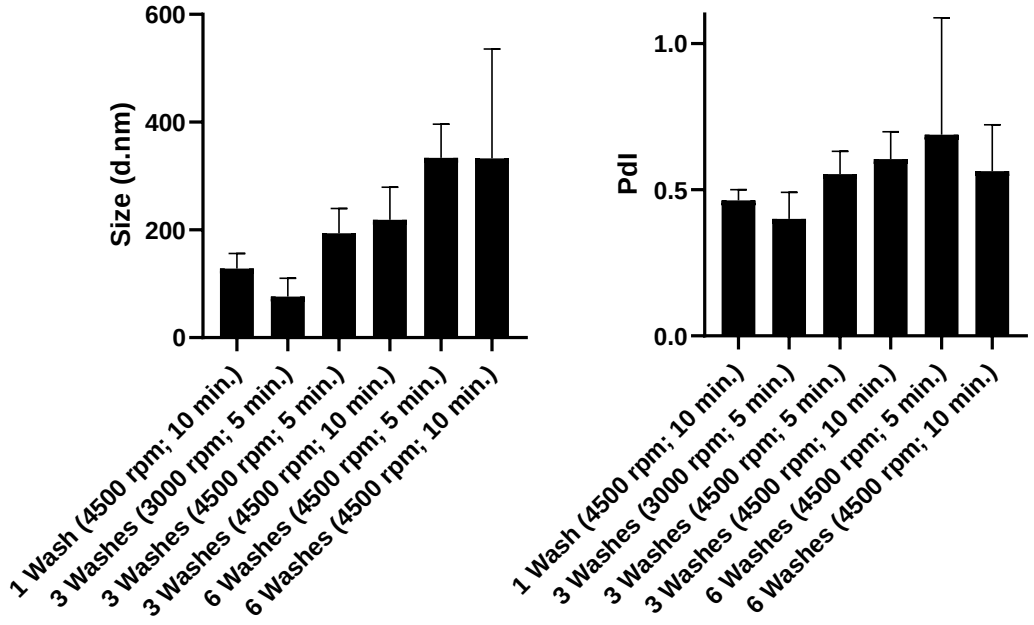

Figure 7 – CaP-NP size (A) and PdI (B) comparison between several washing parameters. Data is presented as mean ± SD for three independent experiments (n=3).

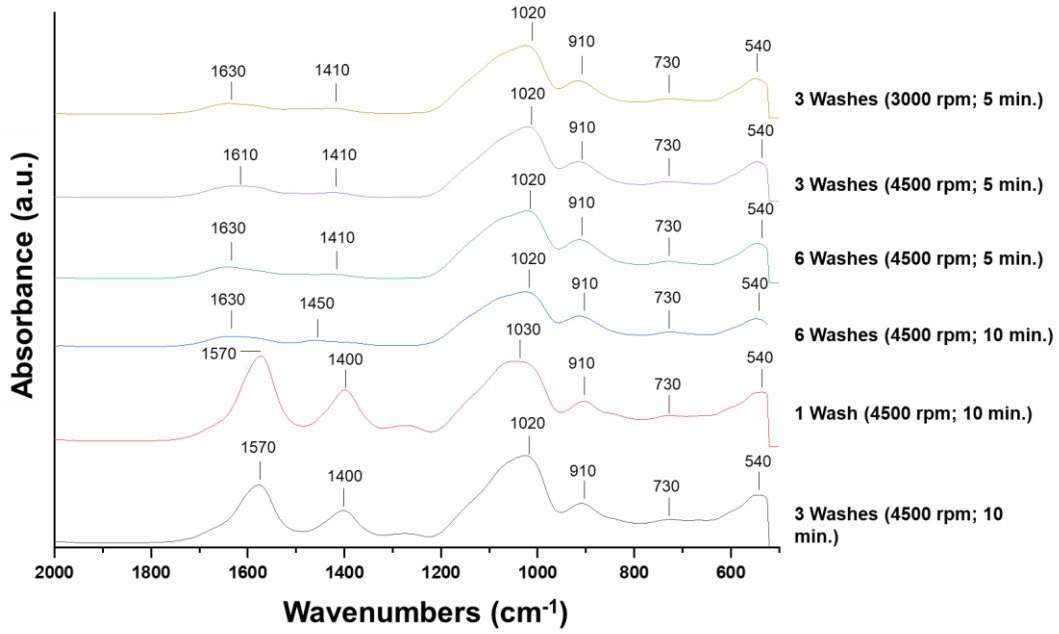

Figure 8 – FTIR analysis between CaP-NPs with different washing parameters.

The findings from the DLS analysis (Table 9 and Figure 7) indicate that only two parameters yield CaP-NPs with sizes below 200 nm. CaP-NPs resulting from a three-wash process (3000 rpm; 5 min) exhibit an average size of 76.34 ± 34.08 nm with a PdI of 0.40 ± 0.09. CaP-NPs resulting from a single wash (4500 rpm; 10 min) display an average size of 156.27 ± 24.81 nm and a PdI of 0.46 ± 0.05.

The chemical characterization of CaP-NPs can be achieved through FTIR spectra analysis. In this regard, CaP-NPs exhibit distinct bands at 550, 910, and 1020 cm^{-1}, attributed to PO_4^{3-} vibrations. The presence of a band at 1410 cm^{-1} signifies CO_3^{2-} vibrations, specifically indicating B-type carbonate substitution where CO_3 occupies PO_4 sites. Furthermore, a band at 1630 cm^{-1} corresponds to citrate ($v_{as}OCO$) vibrations [92, 100].

Upon scrutinizing the chemical composition of CaP-NPs under several washing parameters, as depicted in Figure 8, a noteworthy discrepancy surfaces between the 1 wash (4500 rpm; 10 min) and the 3 washes (4500 rpm; 10 min) conditions, relative to the other spectra. This discrepancy primarily pertains to the citrate and carbonate bands, which exhibit heightened peak intensities. This increase in peak intensity potentially indicates an elevated content of citrate within the CaP-NPs. With the results mentioned above, it is hypothesised that these specific washing parameters are unsuitable for formulating CaP-NPs.

Considering the size increase with the washing steps at higher centrifugation speed, the condition that shows the best result is the CaP-NPs subjected to 3 washes (3000 rpm; 5 min). This formulation exhibits a size below 100 nm, measuring at 76.34 ± 34.08 nm, and possess a charge of – 20.90 ± 0.90 mV. The polydispersity index stands at 0.40 ± 0.09, a parameter that gauges the heterogeneity of the sample and can serve as an indicator of particle aggregation or agglomeration. Samples with values below 0.05 are categorized as monodispersed, while values surpassing 0.70 point to a wide size distribution of particles [101].

4.2 Encapsulation Efficiency

4.2.1 pDNA Encapsulation

Plasmid DNA can be effectively incorporated into CaP-NPs, forming a complex entity referred to as CaP-NP/pDNA. The bonding between pDNA and CaP-NPs is attributed to the electrostatic attraction between the positively charged calcium ions and the negatively charged phosphate groups present in the nucleic acid's backbone [63, 102]. Thus, the encapsulation of pDNA was explored through two distinct methods. Firstly, by introducing pDNA in the precursor calcium solution, and secondly, through adsorption after the CaP-NP formulation. For the adsorption method, the pDNA remained in contact with the CaP-NPs during 4 and 16 h. Thereafter, the formulations were centrifuged and washed three times (3000 rpm for 5 min) and the respective results are presented in Figure 9.

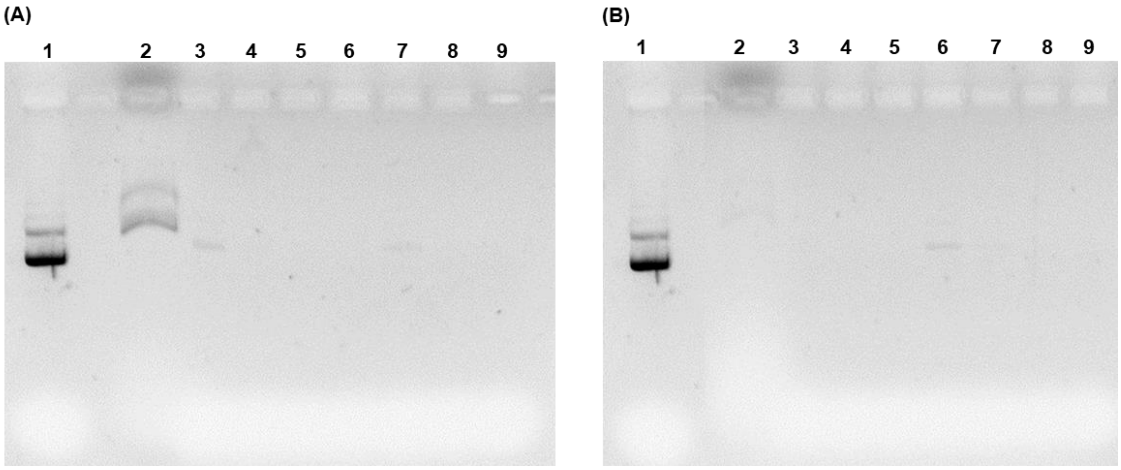

Figure 9 – Analysis of the pDNA encapsulation into CaP-NPs by agarose gel electrophoresis of several supernatants' resultant from the washing process. (A) pDNA added in the calcium precursor solution and through adsorption after the nanoparticles preparation, with an incubation of 4 h. Lane 1 corresponds to pDNA sample and lane 2, 4, 6 and 8 correspond to the supernatant from the several centrifugations of the nanoparticles with pDNA added in the calcium solution. Lane 3, 5, 7 and 9 correspond to the supernatant from the several centrifugations of the nanoparticles with pDNA added through adsorption. (B) pDNA added in the calcium precursor solution and through adsorption after the nanoparticles preparation, with an incubation of 16 h. Lane 1 corresponds to pDNA sample and lane 2, 4, 6 and 8 correspond to the supernatant from the several centrifugations of the nanoparticles with pDNA added in the calcium solution. Lane 3, 5, 7 and 9 correspond to the supernatant from the several centrifugations of the nanoparticles with pDNA added through adsorption.

Figure 9 (A) displays the results for a 4-h incubation period. When pDNA is introduced into the calcium solution, approximately 33 % of the pDNA is lost during the initial centrifugation. Moreover, using this formulation method, only 36 % of the pDNA gets encapsulated within the CaP-NPs. Conversely, when pDNA is added via adsorption, the

encapsulation efficiency reaches approximately 100 %. In the electrophoresis analysis, faint streaks are visible, possibly indicating loss of pDNA in the washing steps, however, these streaks couldn't be precisely detected by the spectrophotometer.

In Figure 9 (B), which represents an overnight incubation, the incorporation of pDNA into the calcium precursor solution yields an encapsulation efficiency of about 73 % within the CaP-NPs. It is worth noting a degree of pDNA loss during both the first and third centrifugations. However, when pDNA is added through adsorption, the encapsulation efficiency achieves 100 %, and there is no discernible loss of pDNA, both qualitatively and quantitatively.

To ensure that the encapsulation of pDNA in CaP-NPs was reproducible, an agarose gel electrophoresis was performed, the results are presented in Figure 10.

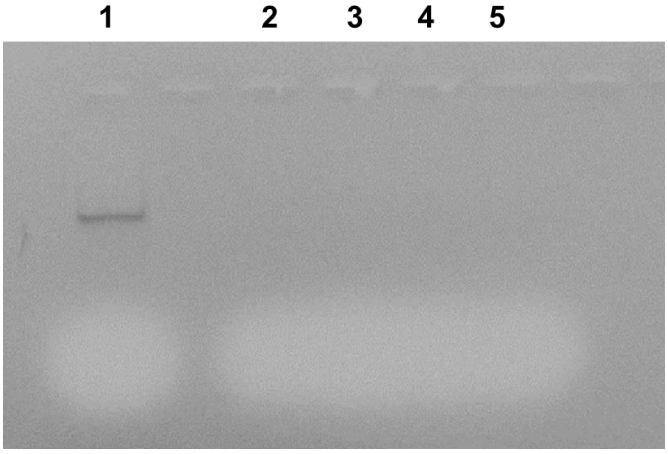

Figure 10 – Analysis of the pDNA encapsulation into NPs by agarose gel electrophoresis of several supernatants resultant from the washing process. Lane 1 corresponds to pDNA sample and lane 2, 3, 4 and 5 corresponds to 4 washing centrifugations.

Based on the aforementioned data, the selected approach for binding pDNA to CaP-NPs was the overnight adsorption method, as evident in Figure 10. Characterization of the CaP-NP/pDNA complexes revealed a size measuring of 133.13 ± 58.12 nm, accompanied by a PdI of 0.65 ± 0.17, the elevated PdI value indicates a wide distribution of particle sizes. The charge of the CaP-NP/pDNA complexes is – 23.70 ± 1.10 mV. When comparing the DLS results, between CaP-NP and CaP-NP/pDNA, a slight increase in size and PdI, and decrease in surface charge, is noticeable. This change could be attributed to the presence of pDNA in the nanoparticles.

Furthermore, to confirm if the pDNA would be encapsulated or adsorbed at the surface, a FTIR analysis was conducted, this result is illustrated in Figure 11.

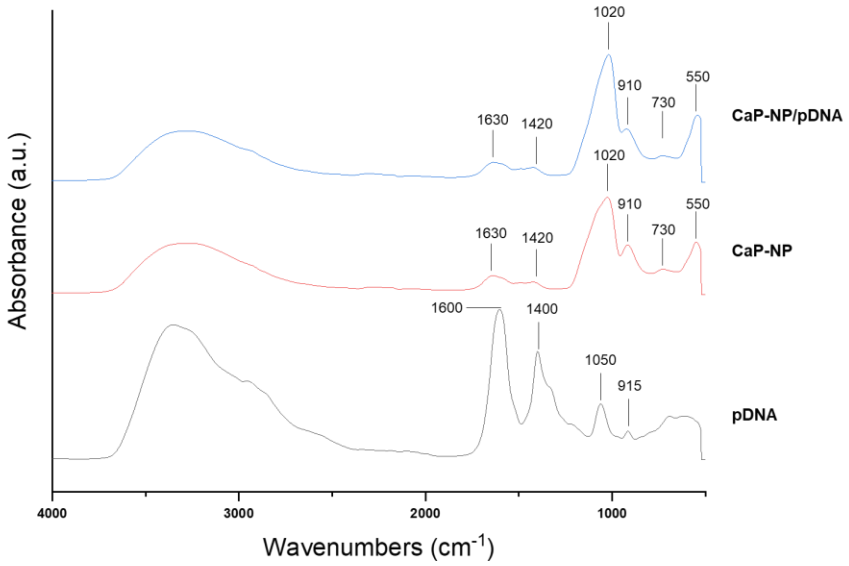

Figure 11 - FTIR spectra of pDNA, CaP-NP and CaP-NP/pDNA for pDNA incubated overnight.

As illustrated in Figure 11, pDNA presents characteristic bands in the 1700-1500 cm^{-1} region could be attributed to nitrogen bases, the band at 1400 cm^{-1} regards the stretching of pyrimidine in DNA. Furthermore, the band at 1050 cm^{-1} could be related to the vibration of ribose (C-C sugar) or associated with stretches in the phosphodiester backbone. Lastly the band at 916 cm^{-1} indicates the presence of pDNA [103, 104]. After comparing and analysing the spectres, it is not possible to confirm the presence of pDNA in CaP-NP/pDNA, since both CaP-NP and pDNA present peaks in the same wavenumbers.

4.2.2 Folic Acid Binding

Nanoparticle targeting systems represent a promising and innovative avenue for pharmaceutical delivery, aiming to mitigate side effects while minimizing unspecific interactions with healthy cells [105]. To functionalize CaP-NPs with folic acid three strategies were outlined. Folic acid was introduced either into the calcium precursor solution (CaP-NP/FACa), into the phosphate precursor solution (CaP-NP/FAPh) and through adsorption (CaP-NP/FAAd).

Initially, a spectral analysis was performed to quantitatively assess folic acid loading, aimed at determining the appropriate wavelength for characterizing the process. As illustrated in Figure 12, folic acid exhibits an absorbance peak at 280 nm.

However, this poses a potential challenge, given that pDNA also absorbs at this wavelength, this is of particular concern since the ultimate objective is to establish CaP-NP/pDNA/FA complexes. Consequently, as a precautionary measure, blank tests involving CaP-NP/FA and CaP-NP/pDNA were conducted during subsequent evaluations of the CaP-NP/pDNA/FA formulation to ensure the absence of any interference.

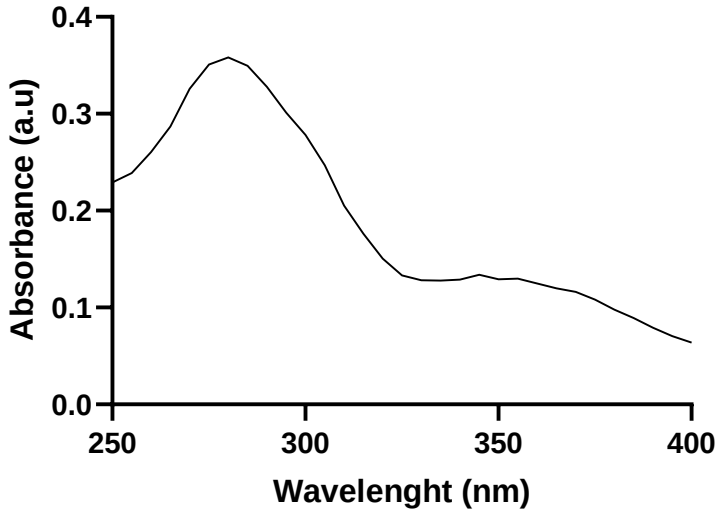

Figure 12 – UV-vis spectra of folic acid.

In the overnight studies, the CaP-NPs that underwent adsorption with folic acid exhibited the highest loading efficiency, reaching approximately 92 %. Subsequently, when folic acid was introduced into the precursor phosphate solution, the loading efficiency was approximately 73 %. Lastly, the incorporation of folic acid into the precursor calcium solution led to a loading efficiency of approximately 70 %.

Conversely, subjecting folic acid to a 24-h contact period resulted in lower loading efficiencies. Folic acid adsorbed in CaP-NPs again presented the higher loading efficiency with approximately 69 %, when folic acid was added to the precursor calcium solution a loading efficiency of approximately 53 %. Finally, when folic acid was added to the phosphate precursor solution a loading efficiency of approximately 44 % was achieved.

Considering the aforementioned outcomes, it is accurate to conclude that the overnight incubation approach allowed higher folic acid adsorption when compared to those obtained over a 24-h period. Furthermore, it is also necessary to ensure that folic acid is present in the nanoparticle's composition. Thus Figure 13, shows the comparison between the several ways in which folic acid was added to the CaP-NPs.

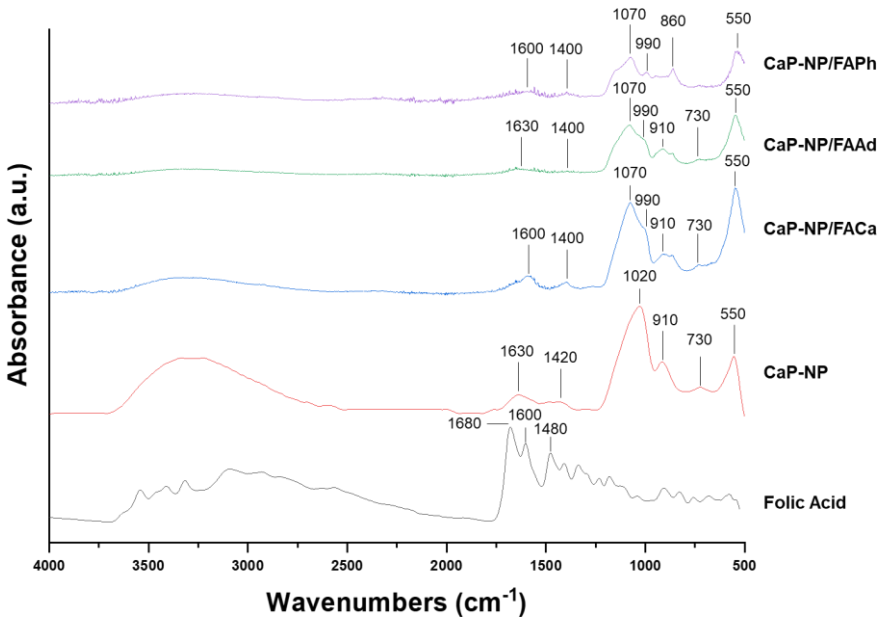

Figure 13 – FTIR spectra of Folic Acid, CaP-NP, CaP-NP/FACa, CaP-NP/FAAd and CaP-NP/FAPh, for folic acid incubated overnight.

Considering Figure 13, folic acid shows characteristic peaks at 1680, 1600 and 1480 cm^{-1}. The band at 1680 cm^{-1} accounts for (C=O) bond stretching vibration of the carboxyl group, while the band at 1600 cm^{-1} corresponds to the bending mode vibration of NH_2 and the band at 1480 cm^{-1} is related to the (-C=C) stretching of phenyl and pterin rings [93, 106].

When comparing to the CaP-NP/FACa spectra to the CaP-NP spectra it is possible to identify a shift in bands at 1600 and 1400 cm^{-1}, to lower wave numbers, indicating an influence from the addition of folic acid [107]. Both the spectra of the CaP-NP/FAPh and of the spectra of the CaP-NP/FAAd show a shift at 1400 cm^{-1} which could as well indicate the presence of folic acid. However, in both of these spectra the presence of folic acid is not as much noticeable when compared to the spectra of the CaP-NP/FACa. These results could indicate that the CaP-NP/FaCa formulation presents higher content of folic acid at the nanoparticles surface.

Based on the outcomes mentioned above, both the CaP-NP/FACa and the CaP-NP/pDNA/FAAd present the most promising results and were chosen for the succeeding tests.

4.2.3 pDNA Encapsulation and Folic Acid Binding

Studies were conducted to ensure that both pDNA and folic acid were able to be conjugated in the CaP-NPs without compromising either loading efficiencies. The approaches chosen were the ones that previously presented the best efficiencies. Taking this into consideration, pDNA an adsorption approach was chosen. For folic acid binding two approaches were outlined, through adsorption after the nanoparticle formulation (the solutions were in contact with the CaP-NP overnight) and through addition in the precursor calcium solution. Figure 14 illustrates the agarose gel electrophoresis of the washing step.

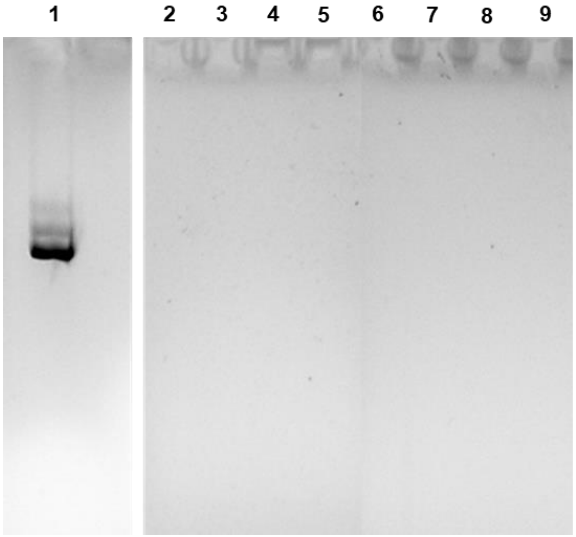

Figure 14 - Analysis of the pDNA encapsulation into CaP-NPs by agarose gel electrophoresis of several supernatants resulting from the washing process. Lane 1 corresponds to pDNA sample. Lane 2, 3, 4 and 5 corresponds to the 4 washing centrifugations of CaP-NP/pDNA/FACa. Lane 6, 7, 8 and 9 corresponds to the 4 washing centrifugations of CaP-NP/pDNA/FAAd.

Figure 14 pertains the agarose gel electrophoresis of the washing step when both pDNA and folic acid are present in the CaP-NPs. This result shows that qualitatively, there is no loss of pDNA in the washing step. To further understand if the folic acid addition would be impacted by the pDNA encapsulation a FTIR spectra was conducted, and its results are present in Figure 15.

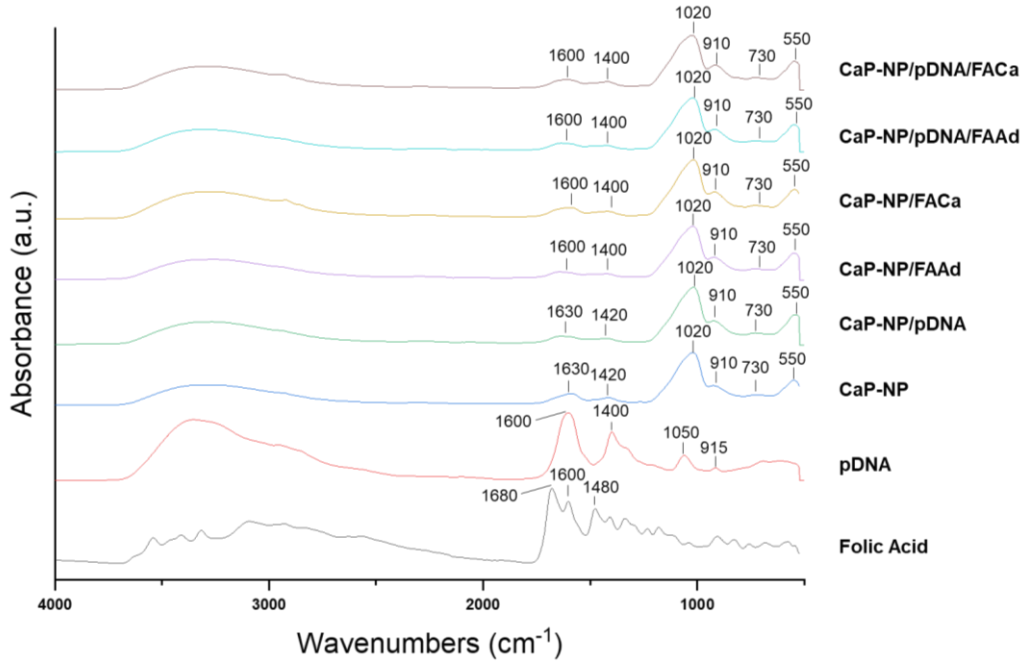

Figure 15 - FTIR spectra of Folic Acid, pDNA, CaP-NP, CaP-NP/pDNA, CaP-NP/FAAd, CaP-NP/FACa, CaP-NP/pDNA/FAAd, CaP-NP/pDNA/FACa.

It is hypothesized that the simultaneous addition of folic acid and pDNA does not influence folic acid loading, since there is no change in the folic acid peaks when comparing the samples with and without pDNA, as showed in Figure 15.

The pDNA encapsulation efficiency and folic acid loading were also assessed in both formulations, as well as the size, PdI and charge was determined by DLS. These results are present in Table 10.

Table 10 - Overview of mean size, PdI, Zeta Potential, folic acid loading efficiency and pDNA encapsulation efficiency for the prepared formulations with pDNA and Folic Acid.

Formulation	Size (nm)	PdI	Zeta Potential (mV)	Folic Acid Loading Efficiency	pDNA Encapsulation Efficiency
CaP-NP/pDNA/FACa	110.42 ± 65.71	0.50 ± 0.07	– 22.20 ± 0.60	73 %	~ 100 %
CaP-NP/pDNA/FAAd	112.63 ± 9.81	0.50 ± 0.22	– 27.40 ± 0.69	99.6 %	~ 100 %

The CaP-NP/pDNA/FAAd showed an efficiency of approximately 100 % for pDNA encapsulation and approximately 99.6 % for folic acid loading. DLS studies show a mean size of 112.63 ± 19.81 nm, with a PdI of 0.50 ± 0.22 and a surface charge of – 27.40 ± 0.69 mV. The CaP-NP/pDNA/FACa formulation presented a pDNA encapsulation efficiency of approximately 100 % and an efficiency of approximately 73 % for the loading of folic acid. Furthermore, DLS results for the CaP-NP/pDNA/FACa present a mean size of 110.42 ± 65.71 nm, with a PdI of 0.50 ± 0.07 and a surface charge of – 22.20 ± 0.60 mV. The qualitative and quantitative results seem to show that none of the molecules were impacted by the coupled loading.

When comparing the surface charge of the CaP-NP/pDNA (– 23.70 ± 1.10 mV) with the systems presenting folic acid, it is important to notice that in CaP-NP/pDNA/FACa (– 22.20 ± 0.60 mV) there is an insignificant change in zeta potential, while CaP-NP/pDNA/FAAd (– 27.40 ± 0.69 mV) presents a noticeable difference. This decrease in the surface charge has been reported before, first by Yang and co-author's and later by Ullah and co-authors and Bandara and co-authors, which suggests that the reduction in surface charge can be due to interactions between the folic acid and the positively charged compounds in the nanoparticles (Ca^{+}) [108–110].

4.3 pDNA Release

The release of pDNA from nanoparticles stands as a pivotal factor in assessing the efficacy of a delivery system. After the formulation process, nanoparticles were incubated at 37 ºC in PBS buffer and samples were taken at different timepoints (30 min, 1, 2, 3, 4, 5 and 6 h). The release of pDNA from the CaP-NP/pDNA was evaluated at two different pH, it was chosen a pH of 7.4, to replicate a healthy tissue environment, and a pH of 5.6 to represent the acidic microenvironment of tumours [111]. Figure 16 represents the cumulative release of curves of pDNA, and Figure 17 illustrates the qualitative release of pDNA, both at two different pHs.

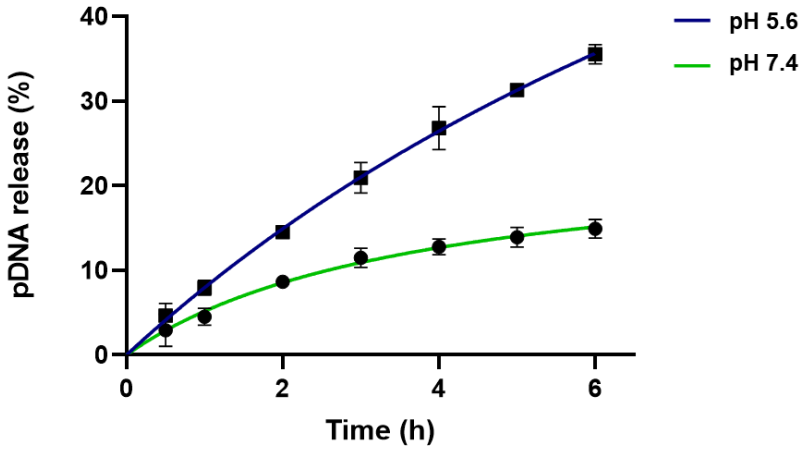

Figure 16 – Cumulative release curves of pDNA encapsulated in CaP-NP/pDNA, in PBS at pH 7.4 and 5.6. Data is presented as mean ± SD for three independent experiments (n=3).

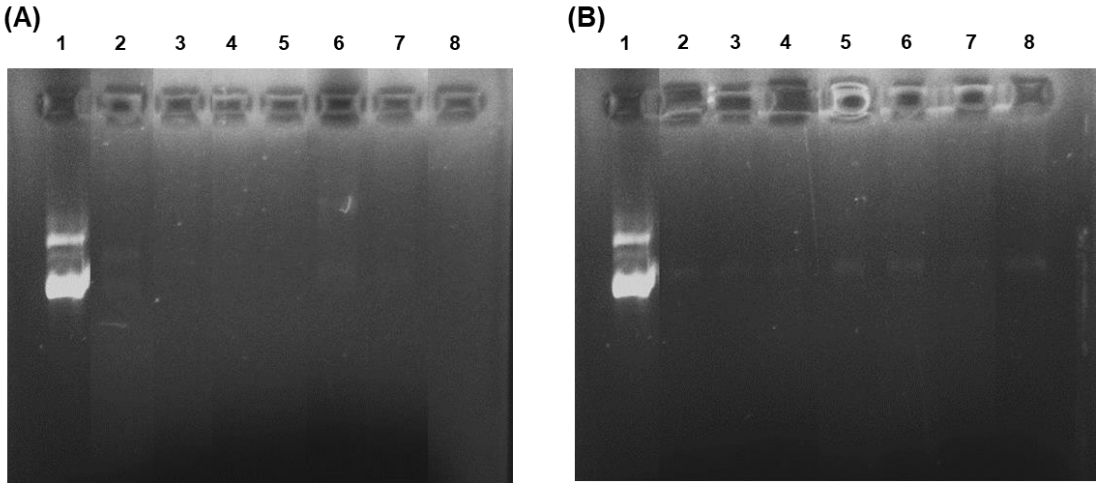

Figure 17 – Analysis of pDNA release from CaP-NP/pDNA by agarose gel electrophoresis through time, in pH 7.4 (A) and pH 5.6 (B). Lane 1 corresponds to pDNA sample and lane 2, 3, 4, 5, 6, 7 and 8 correspond to samples taken at 30 min, 1, 2, 3, 4, 5 and 6 h of incubation in PBS.

As shown in Figure 16, the release rate of pDNA increases with the decrease in pH. The release at pH 7.4 is minimal, around 15 %.

At pH 5.6, a 15 % release is achieved within the initial 2 h, and this proportion surges to over 35 % after a 6 h span, presenting a tendency to reach a plateau of pDNA release. Figure 17 corroborates the previous statement, the agarose gel electrophoresis shows higher release of pDNA at pH 5.6 (Figure 15 (B)), which shows more distinct bands. Furthermore, there is no apparent degradation of pDNA over the incubation period.

The accelerated release rate under pH 5.6 may be ascribed to the electrostatic interaction among the ions within the CaP-NPs. The medium acidity impacts the bonds between the calcium and the phosphate groups, which leads to an increased aqueous solubility of the CaP-NPs as the pH decreases [112].

Moreover, this investigation highlights that the CaP-NPs exhibit the capability to prevent pDNA leakage and enhance stability under physiological pH levels. This characteristic enables swift dissolution in the acidic pH environment of tumours, facilitating the escape from endosomes and the subsequent release of pDNA into the cytoplasm [113]. Bisht *et al.* noted that CaP-NPs are easily dissolved under mildly acidic pH conditions, around pH 5, effectively shielding pDNA from degradation [114].

4.4 *In vitro* Assays

4.4.1 Cell Viability Assays

To assess the systems biocompatibility cell viability assays were conducted. Through the resazurin cell viability or Alamar Blue assay, living cells that are metabolic active can reduce resazurin into a strongly fluorescent dye, resorufin. The fluorescence output is proportional to the number of viable cells [115]. In this assay, two different cell lines were used, a human fibroblast line, and an HPV positive cervical cancer line, HeLa cells. Initially, the cytotoxicity of several concentrations (50, 100, 500 and 1000 μg/mL) of free CaP-NPs systems was evaluated during 24, 48 and 72 h, these results are presented in Figure 18.

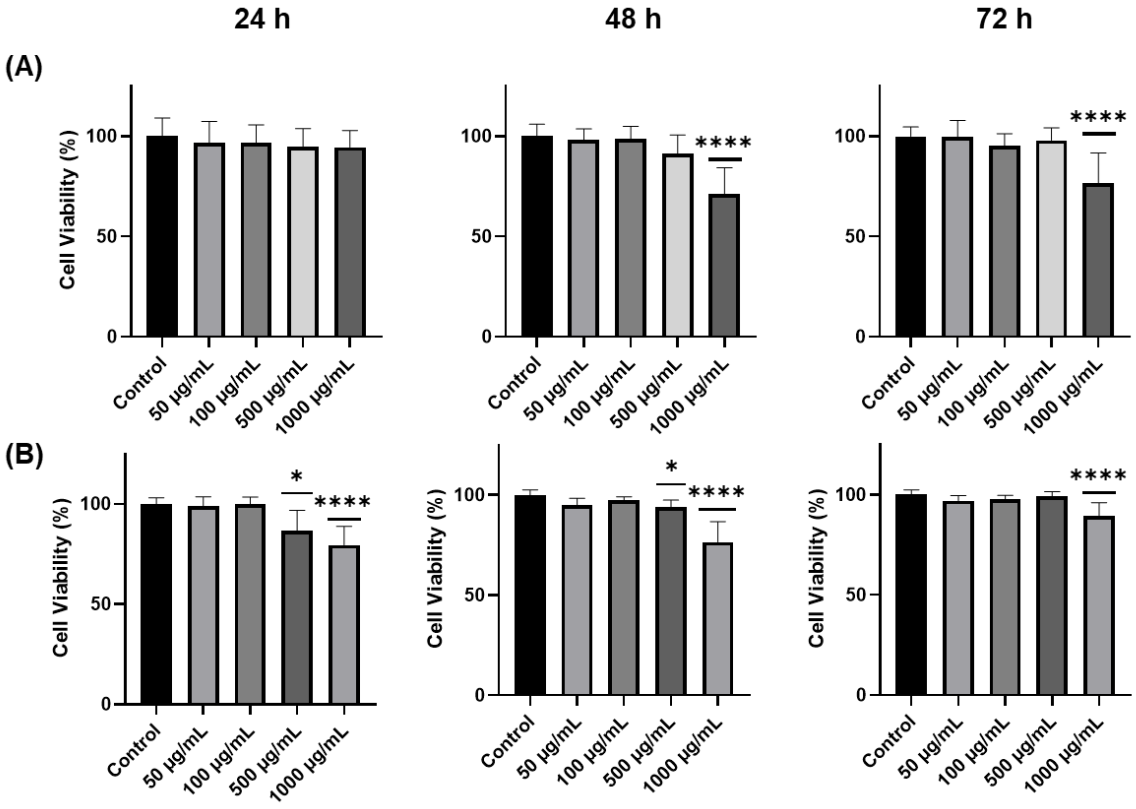

*Figure 18 – Cell viability assay on human fibroblasts (A) and HeLa (B) cells for several concentrations (50, 100, 500 and 1000 µg/mL) of CaP-NPs during a period of incubation of 24, 48 and 72 h. Non-transfected cells were used as negative control. Data is presented as mean ± SD for three independent experiments (n=3) and was analysed by one-way ANOVA. Significance was determined as ****p-value <0.0001 and *p-value < 0.05.*

The outcomes displayed in Figure 18 indicate that high concentrations of CaP-NPs exhibit a reduction in cell viability. Concerning human fibroblasts, solely the 1000 µg/mL concentration presented some cytotoxicity, at 48 and 72 h after transfection (the cell viability rates are 71 % and 76 %, respectively). For both the 500 µg/mL and 1000 µg/mL concentrations show diminished cell viability, but only the concentration of 1000 µg/mL shows cytotoxicity at 24 and 48 h (the cell viability rates are 79.5 % and 76.5 %, respectively). It is important to highlight that any values at or below 80 % are categorized as cytotoxic [116].

Based on the aforementioned results, a CaP-NP concentration of 100 µg/mL has been selected for subsequent studies, as it does not exhibit any cytotoxic effects, maintaining viability levels above 95 %. A CaP-NP concentration of 100 µg/mL was used for further cell tests. A cell viability assay was also conducted using nanoparticles with pDNA and or folic acid, these results are presented in Figure 19.

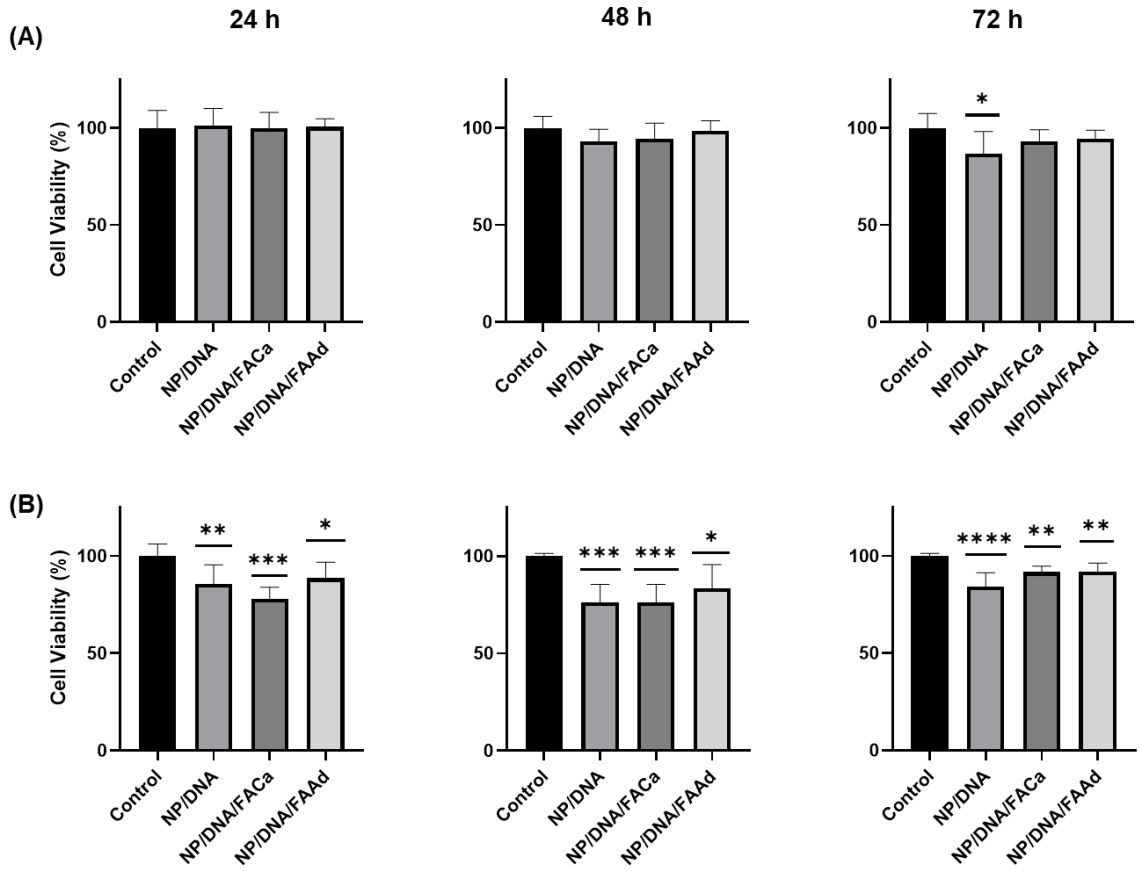

*Figure 19 – Cell viability assay on human fibroblasts (A) and HeLa (B) cells treated with CaP-NP/pDNA, CaP-NP/pDNA/FACa and CaP-NP/pDNA/FAAd for a period of incubation of 24, 48 and 72 h. Non-transfected cells were used as negative control. Data is presented as mean ± SD for three independent experiments (n=3) and was analysed by one-way ANOVA. Significance was determined as ****p-value <0.001, ***p-value < 0.001, **p-value < 0.01 and *p-value < 0.05.*

Figure 19 depicts the cell viability outcomes of the CaP-NP complex when loaded with pDNA, or with pDNA and folic acid. The human fibroblasts are viable in the presence of the developed formulations, during the experiment. A reduced cell viability is observed after 72 h in contact with the CaP-NP/pDNA formulation. Nevertheless, the cancer cell viability is reduced when in contact with the prepared formulations, during 72 h of experiment.

At 24 h the CaP-NP/pDNA/FACa exhibits the greatest impact, decreasing cell viability to approximately 77 %. This outcome could be attributed to the presence of folic acid in the delivery systems, which leads to higher internalization rates in cancer cells presenting folic acid receptors [117]. Only at the 48-h mark does CaP-NP/pDNA, lacking a ligand, attain a viability rate of 76 %. To better understand how the systems are internalized, the NPs uptake was evaluated through Confocal Microscopy.

4.4.2 Cell Internalization Assay

Laser confocal microscopy was used to analyse FITC marked CaP-NP cellular uptake in fibroblast and HeLa cells, with VECTASHIELD labelled nucleus. Figure 20 illustrates the internalization of CaP-NP 2 h after transfection.

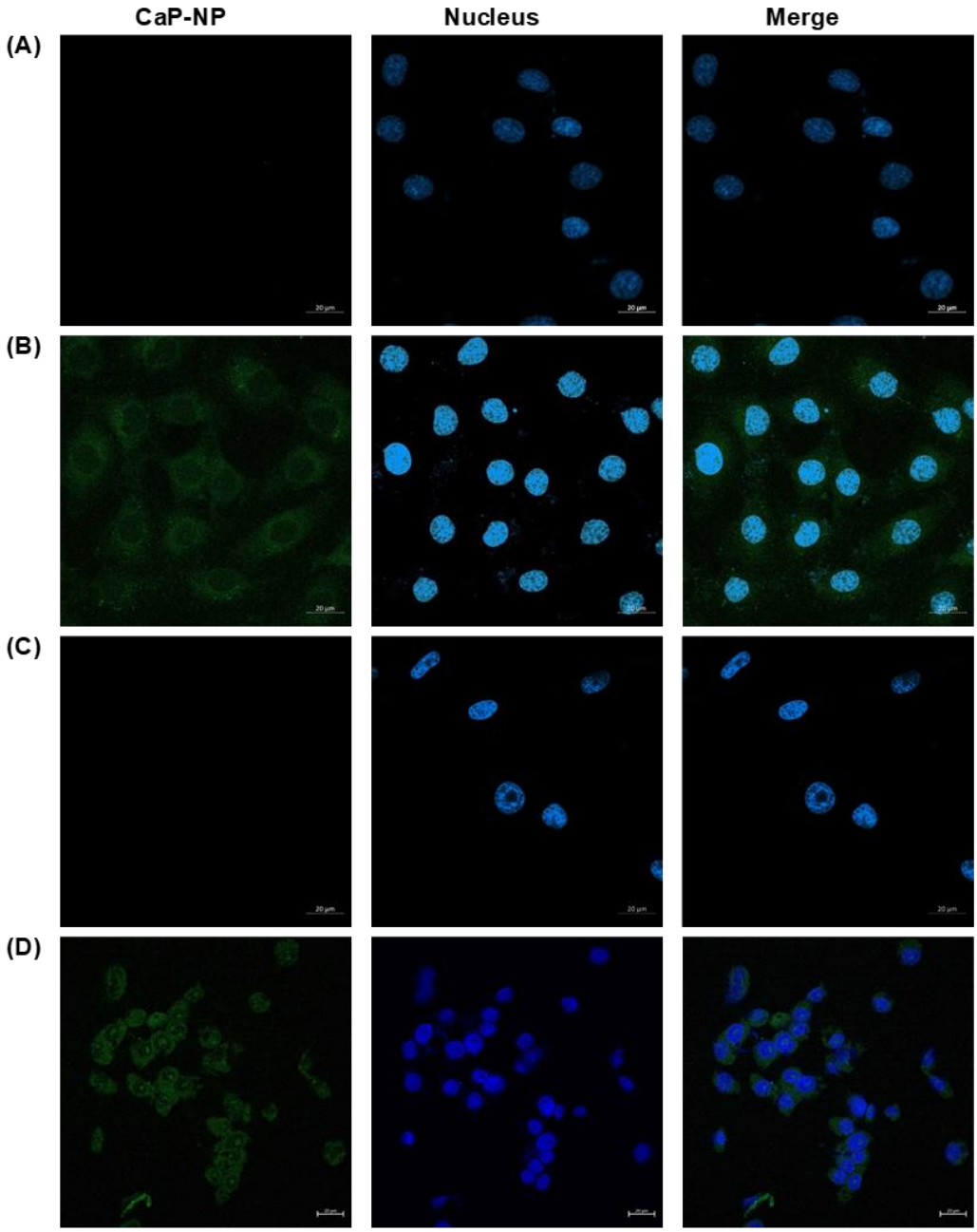

Figure 20 – Confocal microscopy images of Fibroblast cells, (A) non-transfected cells and (B) cells transfected with CaP-NP. Images of HeLa cells, (C) non-transfected cells and (D) cells transfected with CaP-NP, 2 h after transfection. The nuclei were stained with VECTASHIELD, and the CaP-NP were marked with FITC.

The results obtained from the fibroblast cells demonstrate that the nanoparticles readily transverse the cell membrane and accumulate within the cell's cytoplasm. In the case of HeLa cells, the results seem to indicate that the CaP-NPs easily internalize and can reach the cell nucleus. Upon comparing the outcomes from the different cell lines, it appears that both can easily internalize CaP-NPs, and the results from HeLa cells suggest that there is greater uptake of CaP-NPs. This observation aligns with prior research findings. Pedraza *et al.* reported that CaP-NP transfection in the fibroblast cell line was less effective in comparison to an osteoblastic cell line, although CaP-NPs were readily internalized in both lines [118]. Additionally, Sokolova *et al.* demonstrated that CaP-NP are more efficiently taken up by HeLa cells when compared to fibroblastic cells, particularly in a two-dimensional monoculture setting [119].

In the aforementioned cell viability results, no significant difference was observed between the several formulations (CaP-NP; CaP-NP/pDNA; CaP-NP/pDNA/FACa; CaP-NP/pDNA/FAAd). Thus, an internalization assay was performed in HeLa cells. Figure 21 depicts a comparison of internalization between free nanoparticles, nanoparticles with the incorporation of pDNA and nanoparticles functionalized with folic acid in two different approaches.

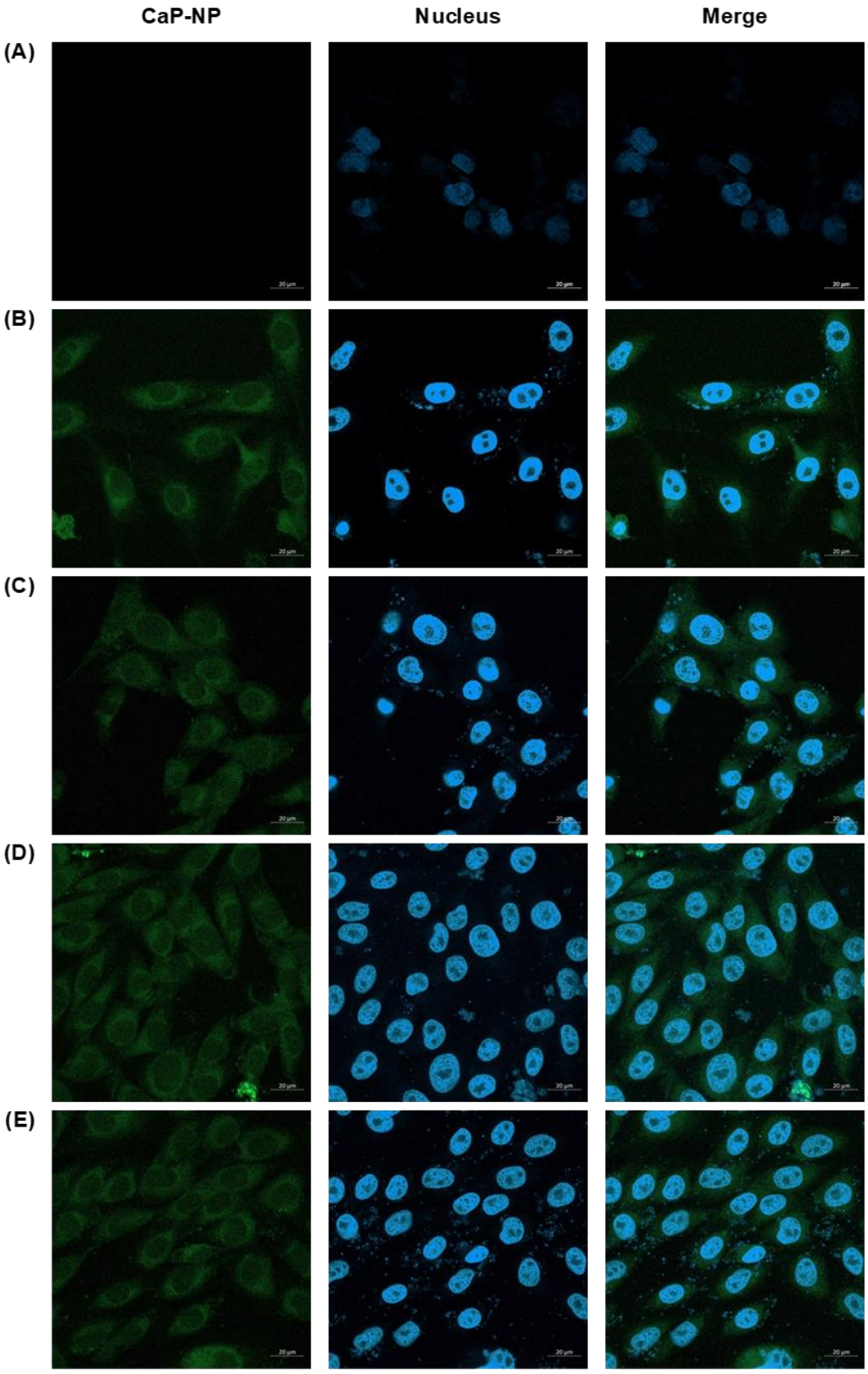

Figure 21 - Confocal microscopy images of HeLa cells 30 min after transfection. (A) Non-transfected HeLa cells, (B) CaP-NP, (C) CaP-NP/pDNA, (D) CaP-NP/pDNA/FACa and (E) CaP-NP/pDNA/FAAd. The nuclei were stained with VECTASHIELD, and the nanoparticles were marked with FITC.

The introduction of folic acid on the nanoparticle surface enables the targeting of cancer cells presenting folate receptors [117]. In this context, Figure 21 compares internalization efficiency between the several formulated systems after 30 min. The results indicate that both CaP-NP and CaP-NP/pDNA present the lowest amount of cell internalization. Conversely, CaP-NP/pDNA/FACa and CaP-NP/pDNA/FAAd formulations appear to exhibit higher concentration of NPs inside the cells. Thus, both these systems show the ability to penetrate the cell membrane and deliver the pDNA to the cytoplasm. Literature proposes that when these systems are internalized through endocytosis, the disassociation of the constituent ions (Ca^{2+} and PO_4^{3-}) leads to an increase of osmotic pressure, causing the expansion and rupture of the vesicle, releasing the therapeutic agent, Ca^{2+} and PO_4^{3-} into the cytoplasm [65, 86]. After pDNA reaches the nucleus, it is hypothesized that transcription occurs and p53 is expressed.

4.4.3 p53 Gene Expression

Following the transfection of fibroblasts and HeLa cells with CaP-NP/pDNA, both with and without folic acid, the p53 gene expression was assessed. In the first place, the RNA extraction was conducted, then the RNA was reversed transcribed to obtain cDNA, and lastly RT-PCR was performed to amplify the p53 gene, employing specific primers. The products of RT-PCR were qualitatively analysed through a 1 % agarose gel electrophoresis. Non-transfected cells were used as a control and a negative control, composed of every PCR reagent and without cDNA, was applied to detect any potential contaminations. The results in Figure 22 show the outcome of the RT-PCR in both cell lines.

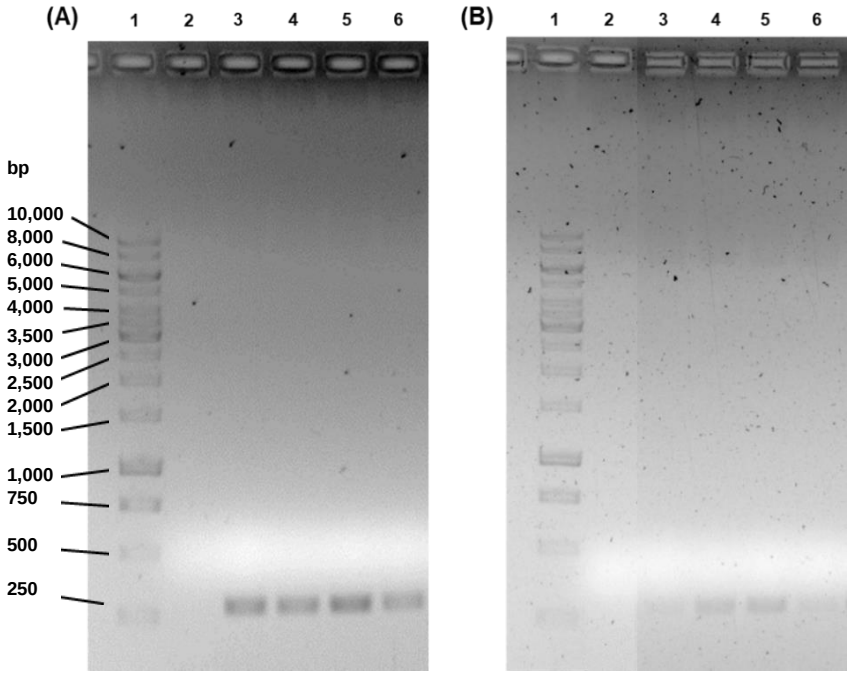

Figure 22 - Analysis of RT-PCR products by agarose gel electrophoresis. Evaluation of p53 transcripts in fibroblast cells (A) and HeLa cells (B). Lane 1 corresponds to DNA molecular weight marker, lane 2 corresponds to the negative control, which is composed of every PCR reagent except cDNA, lane 3 corresponds to non-transfected cells, lane 4 corresponds to cells transfected with CaP-NP/pDNA, lane 5 corresponds to cells transfected with CaP-NP/pDNA/FACa and lane 6 corresponds to cells transfected with CaP-NP/pDNA/FAAd.

Firstly, it is important to acknowledge that no contamination is evident in both negative controls. In the case of fibroblast cells, the results suggest that the p53 gene expression is similar when comparing the non-transfected with the transfected cells. This result seems indicative that the nanoparticles do not inflict alterations in healthy cells. The HeLa cells results show that p53 expression is barely detectable in non-transfected cells. However, when cells are transfected with CaP-NP/pDNA and CaP-NP/pDNA/FACa it seems that there is an increase in gene expression, with the latter approach exhibiting a prominent band. Conversely, the CaP-NP/pDNA/FAAd does not show a great significance when compared to the non-transfected cells. This tendency could be attributed to the fact that both pDNA and folic acid are adsorbed to the NPs surface during simultaneous incubation. During this process, the folic acid can compete with pDNA by the available positive binding sites on the NPs surface. This suggestion can justify the lower content of pDNA inside the cells (considering the low p53 transcript levels) and the high folic acid loading determined in the topic 4.2.3.

These results are indicative that both CaP-NP/pDNA and CaP-NP/pDNA/FACa formulations present favourable protection and delivery of the pDNA to the cancer cells.

Furthermore, both formulations can induce the desired effect, resulting in the increase of p53 expression levels. To best of our knowledge, no previous work has been described as delivering pDNA to cancer cells through CaP-NPs functionalized with folic acid.

Chapter 5 – Conclusions and Future Perspectives

Cervical cancer, primarily caused by persistent infection with high-risk strains of HPV, poses a significant and urgent global health challenge, particularly in low- and middle-income nations. Despite being one of the most preventable and treatable forms of cancer, cervical cancer continues to rank as a leading cause of cancer-related mortality among women. In the ongoing battle against cervical cancer, plasmid DNA-based treatments have emerged as a promising frontier. Plasmid DNA, a small, circular genetic material, can be genetically engineered to carry therapeutic genes to combat cancer cells. However, it is crucial to acknowledge that plasmid DNA is susceptible to degradation by various agents. Consequently, it becomes imperative to explore efficient methods of encapsulating plasmid DNA to ensure its safe and effective delivery to cancer cells.

Herein, the focus was the development of plasmid DNA-loaded calcium phosphate nanoparticles functionalized with folic acid for a targeted delivery in HPV positive cancer cells. Thus, these delivery systems were optimized to ensure the best characteristics, such as size, PdI and surface charge. The most favourable outcome for the CaP-NPs presented a size of 76.34 ± 34.08 nm, with a PdI of 0.40 ± 0.09 and a charge of – 20.90 ± 0.90 mV. Furthermore, several methods were delineated to encapsulate plasmid DNA, which was through overnight adsorption. The final CaP-NP/pDNA formulation revealed a size measuring 133.13 ± 58.12 nm, accompanied by a PdI of 0.65 ± 0.17 with a surface charge of – 23.70 ± 1.10 mV. Functionalization of these NPs with folic acid was also optimized, and several approaches were tried. In the end, two methods were chosen, CaP-NP/FACa and CaP-NP/FAAd, which exhibited a folic acid loading efficiency of approximately 92 and 70 %, respectively. Then, the formulations were also characterized in the presence of both pDNA and folic acid. The CaP-NP/pDNA/FAAd showed an efficiency of approximately 100 % for pDNA and approximately 99.6 % for folic acid, and DLS results showed a mean size of 112.63 ± 19.81 nm, with a PdI of 0.50 ± 0.22 and a surface charge of – 27.40 ± 0.69 mV. The CaP-NP/pDNA/FACa presented an adsorption efficiency of pDNA in the nanoparticles of 100 % and the loading of approximately 73 % of folic acid. Furthermore, DLS results for the CaP-NP/pDNA/FACa present a mean size of 110.42 ± 65.71 nm, with a PdI of 0.50 ± 0.07 and a surface charge of – 22.20 ± 0.60 mV. Through all the optimizations the formulations were chemically characterized through FTIR, to ensure the presence of folic acid.

In vitro assays were carried out, and the CaP-NPs did not show great inherent cytotoxicity, although it is important to notice that the decrease in viability is time and

concentration dependent. Furthermore, when the pDNA and the folic acid were added, the delivery systems did not affect healthy cells but decreased the viability in the cancer cell line. Transfection efficiency was evaluated, and the nanoparticles showed an easy entry and accumulation within the cells, with higher uptake in the cancer cell line. To ensure that the pDNA reached the nucleus the p53 transcripts were evaluated by PCR and the results showed an increased expression values when the cancer cell line was transfected with both CaP-NP/pDNA and CaP-NP/pDNA/FACa.

The present work demonstrated that the formulated delivery systems can be considered as promising vehicles to deliver pDNA. However, these systems could be further optimized to ensure a higher impact in the cancer cell viability, such as adding polymers to its formulation to ensure lower degradation. This work was the first step of contact of CaP-NPs as nanodevices for cervical cancer, further assays should be conducted to better understand this delivery system. For example, Carbon, Hydrogen and Nitrogen (CHN) chemical analysis, thermogravimetric analysis, and X-ray photoelectron spectroscopy. Further *in vitro* studies could also be carried out, such as an apoptosis assay, to understand the apoptotic response, and a western blot to further consolidate the p53 expression results previously obtained.

The present study showed the possibility to formulate several CaP-NPs, loaded with pDNA and functionalized with folic acid, which exhibit relevant properties, warranting their further investigation as therapeutics for cervical cancer.

Chapter 6 – References

[1] L. Ferrall, K. Y. Lin, R. B. S. Roden, C. F. Hung, and T. C. Wu, "Cervical cancer immunotherapy: Facts and hopes," *Clinical Cancer Research*, vol. 27, no. 18, pp. 4953–4973, 2021, doi: 10.1158/1078-0432.CCR-20-2833.

[2] S. Gupta and M. K. Gupta, "Possible role of nanocarriers in drug delivery against cervical cancer," *Nano Rev Exp*, vol. 8, no. 1, p. 1335567, 2017, doi: 10.1080/20022727.2017.1335567.

[3] C.A. Burmeister, S.F. Khan, G. Schäfer, N. Mbatani, T. Adams, J. Moodley and S. Prince, "Cervical cancer therapies: Current challenges and future perspectives," *Tumour Virus Research*, vol. 13. Elsevier B.V., Jun. 01, 2022. doi: 10.1016/j.tvr.2022.200238.

[4] R. Wang, W. Pan, L. Jin, W. Huang, Y. Li, D. Wu, C. Gao, D. Ma and S. Liao, "Human papillomavirus vaccine against cervical cancer: Opportunity and challenge," *Cancer Lett*, vol. 471, no. September 2019, pp. 88–102, 2020, doi: 10.1016/j.canlet.2019.11.039.

[5] P. Zhou, W. Liu, Y. Cheng, and D. Qian, "Nanoparticle-based applications for cervical cancer treatment in drug delivery, gene editing, and therapeutic cancer vaccines," *Wiley Interdiscip Rev Nanomed Nanobiotechnol*, vol. 13, no. 5, pp. 1–15, 2021, doi: 10.1002/wnan.1718.

[6] V. Tomaić, "Functional roles of E6 and E7 oncoproteins in HPV-induced malignancies at diverse anatomical sites," *Cancers (Basel)*, vol. 8, no. 10, 2016, doi: 10.3390/cancers8100095.

[7] A. Pal and R. Kundu, "Human Papillomavirus E6 and E7: The Cervical Cancer Hallmarks and Targets for Therapy," *Front Microbiol*, vol. 10, no. January, 2020, doi: 10.3389/fmicb.2019.03116.

[8] K. Munger, "Papillomaviruses," in *Encyclopedia of Cancer*, Elsevier, 2018, pp. 212–218. doi: 10.1016/B978-0-12-801238-3.98745-2.

[9] A. M. Almeida, J. A. Queiroz, F. Sousa, and Â. Sousa, "Cervical cancer and HPV infection: ongoing therapeutic research to counteract the action of E6 and E7 oncoproteins," *Drug Discov Today*, vol. 24, no. 10, pp. 2044–2057, Oct. 2019, doi: 10.1016/j.drudis.2019.07.011.

[10] S. v. Graham, “Human papillomavirus: Gene expression, regulation and prospects for novel diagnostic methods and antiviral therapies,” *Future Microbiology*, vol. 5, no. 10. pp. 1493–1506, Oct. 2010. doi: 10.2217/fmb.10.107.

[11] N. A. Wallace and D. A. Galloway, “Novel Functions of the Human Papillomavirus E6 Oncoproteins,” *Annu Rev Virol*, vol. 2, pp. 403–423, 2015, doi: 10.1146/annurev-virology-100114-055021.

[12] C. A. Moody and L. A. Laimins, “Human papillomavirus oncoproteins: Pathways to transformation,” *Nat Rev Cancer*, vol. 10, no. 8, pp. 550–560, 2010, doi: 10.1038/nrc2886.

[13] J. Doorbar, N. Egawa, H. Grif, and C. Kranjec, “Human papillomavirus molecular biology and disease association,” pp. 2–23, 2016, doi: 10.1002/rmv.

[14] S. v. Graham, “The human papillomavirus replication cycle, and its links to cancer progression: A comprehensive review,” *Clin Sci*, vol. 131, no. 17, pp. 2201–2221, 2017, doi: 10.1042/CS20160786.

[15] E.-K. Yim and J.-S. Park, “The Role of HPV E6 and E7 Oncoproteins in HPV-associated Cervical Carcinogenesis,” *Cancer Res Treat*, vol. 37, no. 6, p. 319, 2005, doi: 10.4143/crt.2005.37.6.319.

[16] S. B. vande Pol and A. J. Klingelhutz, “Papillomavirus E6 oncoproteins,” *Virology*, vol. 445, no. 1–2, pp. 115–137, 2013, doi: 10.1016/j.virol.2013.04.026.

[17] S. Beaudenon and J. M. Huibregtse, “HPV E6, E6AP and cervical cancer,” *BMC Biochem*, vol. 9, no. SUPPL. 1, pp. 1–7, 2008, doi: 10.1186/1471-2091-9-S1-S4.

[18] M. E. McLaughlin-Drubin and K. Munger, “Papillomaviruses,” in *Reference Module in Biomedical Sciences*, Elsevier, 2014. doi: 10.1016/B978-0-12-801238-3.00007-6.

[19] B. Zhang, W. Chen, and A. Roman, “The E7 proteins of low- and high-risk human papillomaviruses share the ability to target the pRB family member p130 for degradation,” *Proc Natl Acad Sci U S A*, vol. 103, no. 2, pp. 437–442, 2006, doi: 10.1073/pnas.0510012103.

[20] X. Zhao, W. Sun, Y. Ren, and Z. Lu, “Therapeutic potential of p53 reactivation in cervical cancer,” *Critical Reviews in Oncology/Hematology*, vol. 157. Elsevier Ireland Ltd, Jan. 01, 2021. doi: 10.1016/j.critrevonc.2020.103182.

[21] T. Ozaki and A. Nakagawara, “Role of p53 in cell death and human cancers,” *Cancers*, vol. 3, no. 1. pp. 994–1013, Mar. 2011. doi: 10.3390/cancers3010994.

[22] B. P. Bouchet, C. C. de Fromentel, A. Puisieux, and C. M. Galmarini, “p53 as a target for anti-cancer drug development,” *Critical Reviews in Oncology/Hematology*, vol. 58, no. 3. Elsevier Ireland Ltd, pp. 190–207, 2006. doi: 10.1016/j.critrevonc.2005.10.005.

[23] C. Hidai and H. Kitano, “Nonviral Gene Therapy for Cancer: A Review,” *Diseases*, vol. 6, no. 3, p. 57, Jul. 2018, doi: 10.3390/diseases6030057.

[24] C. L. Hardee, L. M. Arévalo-Soliz, B. D. Hornstein, and L. Zechiedrich, “Advances in non-viral DNA vectors for gene therapy,” *Genes*, vol. 8, no. 2. MDPI AG, Feb. 01, 2017. doi: 10.3390/genes8020065.

[25] D. Ibraheem, A. Elaissari, and H. Fessi, “Gene therapy and DNA delivery systems,” *International Journal of Pharmaceutics*, vol. 459, no. 1–2. pp. 70–83, Jan. 01, 2014. doi: 10.1016/j.ijpharm.2013.11.041.

[26] D. M. F. Prazeres, G. N. M. Ferreira, G. A. Monteiro, C. L. Cooney, and J. M. S. Cabral, “Large-scale production of pharmaceutical-grade plasmid DNA for gene therapy: problems and bottlenecks,” *Trends Biotechnol*, vol. 17, no. 4, pp. 169–174, Apr. 1999, doi: 10.1016/S0167-7799(98)01291-8.

[27] T. Wirth, N. Parker, and S. Ylä-Herttuala, “History of gene therapy,” *Gene*, vol. 525, no. 2, pp. 162–169, Aug. 2013, doi: 10.1016/j.gene.2013.03.137.

[28] S. Yıldırım and F. Kocabaş, “Gene Therapy Products Reached to Market by 2021,” *Gene Editing*, vol. 2, no. 2, pp. 1–21, 2021, doi: 10.29228/genediting.54101.

[29] “Gene Therapy Clinical Trials Worldwilde.” Accessed: Jan. 11, 2023. [Online]. Available: https://a873679.fmphost.com/fmi/webd/GTCT

[30] A. R. Lara and O. T. Ramírez, “Plasmid DNA production for therapeutic applications,” *Methods in Molecular Biology*, vol. 824, pp. 271–303, 2012, doi: 10.1007/978-1-61779-433-9_14.

[31] S. Gupta and L. Yel, “Molecular Biology and Genetic Engineering,” in *Middleton’s Allergy*, Elsevier, 2014, pp. 162–183. doi: 10.1016/B978-0-323-08593-9.00011-5.

[32] J. Pahle and W. Walther, “Vectors and strategies for nonviral cancer gene therapy,” *Expert Opinion on Biological Therapy*, vol. 16, no. 4. Taylor and Francis Ltd, pp. 443–461, Apr. 02, 2016. doi: 10.1517/14712598.2016.1134480.

[33] Y. Liu, S. Musetti, and L. Huang, “Gene Therapy with Plasmid DNA,” in *Burger’s Medicinal Chemistry and Drug Discovery*, Wiley, 2021, pp. 1–35. doi: 10.1002/0471266949.bmc073.pub3.

[34] A. Abdulrahman and A. Ghanem, “Recent advances in chromatographic purification of plasmid DNA for gene therapy and DNA vaccines: A review,” *Analytica Chimica Acta*, vol. 1025. Elsevier B.V., pp. 41–57, Sep. 26, 2018. doi: 10.1016/j.aca.2018.04.001.

[35] J. Mairhofer and R. Grabherr, “Rational vector design for efficient non-viral gene delivery: Challenges facing the use of plasmid DNA,” in *Molecular Biotechnology*, Jun. 2008, pp. 97–104. doi: 10.1007/s12033-008-9046-7.

[36] N. Bono, F. Ponti, D. Mantovani, and G. Candiani, “Non-viral in vitro gene delivery: It is now time to set the bar!,” *Pharmaceutics*, vol. 12, no. 2. MDPI AG, Feb. 01, 2020. doi: 10.3390/pharmaceutics12020183.

[37] G. N. M. Ferreira, G. A. Monteiro, D. M. F. Prazeres, and J. M. S. Cabral, “Downstream processing of plasmid DNA for gene therapy and DNA vaccine applications,” *Trends Biotechnol*, vol. 18, no. 9, pp. 380–388, Sep. 2000, doi: 10.1016/S0167-7799(00)01475-X.

[38] A. Carnes and J. Williams, “Plasmid DNA Manufacturing Technology,” *Recent Pat Biotechnol*, vol. 1, no. 2, pp. 151–166, Jun. 2007, doi: 10.2174/187220807780809436.

[39] G. N. M. Ferreira, “Chromatographic Approaches in the Purification of Plasmid DNA for Therapy and Vaccination,” *Chem Eng Technol*, vol. 28, no. 11, pp. 1285–1294, Nov. 2005, doi: 10.1002/ceat.200500158.

[40] Â. Sousa, F. Sousa, and J. A. Queiroz, “Advances in chromatographic supports for pharmaceutical-grade plasmid DNA purification,” *J Sep Sci*, vol. 35, no. 22, pp. 3046–3058, Nov. 2012, doi: 10.1002/jssc.201200307.

[41] M. M. Diogo, J. A. Queiroz, and D. M. F. Prazeres, “Chromatography of plasmid DNA,” *J Chromatogr A*, vol. 1069, no. 1, pp. 3–22, Mar. 2005, doi: 10.1016/j.chroma.2004.09.050.

[42] J. Stadler, R. Lemmens, and T. Nyhammar, “Plasmid DNA purification,” *J Gene Med*, vol. 6, no. S1, pp. S54–S66, Feb. 2004, doi: 10.1002/jgm.512.

[43] A. Ghanem, R. Healey, and F. G. Adly, “Current trends in separation of plasmid DNA vaccines: A review,” *Anal Chim Acta*, vol. 760, pp. 1–15, Jan. 2013, doi: 10.1016/j.aca.2012.11.006.

[44] A. Abdulrahman and A. Ghanem, “Recent advances in chromatographic purification of plasmid DNA for gene therapy and DNA vaccines: A review,” *Anal Chim Acta*, vol. 1025, pp. 41–57, Sep. 2018, doi: 10.1016/j.aca.2018.04.001.

[45] K. Lundstrom, “Viral Vectors in Gene Therapy,” *Diseases*, vol. 6, no. 2, p. 42, May 2018, doi: 10.3390/diseases6020042.

[46] Y. K. Sung and S. W. Kim, “Recent advances in the development of gene delivery systems,” *Biomaterials Research*, vol. 23, no. 1. BioMed Central Ltd., Mar. 12, 2019. doi: 10.1186/s40824-019-0156-z.

[47] M. Sainz-Ramos, I. Gallego, I. Villate-Beitia, J. Zarate, I. Maldonado, G. Puras and J.L. Pedraz, “How far are non-viral vectors to come of age and reach clinical translation in gene therapy?,” *International Journal of Molecular Sciences*, vol. 22, no. 14. MDPI AG, Jul. 02, 2021. doi: 10.3390/ijms22147545.

[48] S. Patil, Y. Gao, X. Lin, Y. Li, K. Dang, Y. Tian, W. Zhang, S. Jiang, A. Qadir and A. Qian, “The development of functional non-viral vectors for gene delivery,” *Int J Mol Sci*, vol. 20, no. 21, Nov. 2019, doi: 10.3390/ijms20215491.

[49] M. Butt, M. Zaman, A. Ahmad, R. Khan, T. Mallhi, M. Hasan, Y. Khan, S. Hafeez, E. Massoud, Md. Rahman and S. Cavalu, “Appraisal for the Potential of Viral and Nonviral Vectors in Gene Therapy: A Review,” *Genes*, vol. 13, no. 8. MDPI, Aug. 01, 2022. doi: 10.3390/genes13081370.

[50] M. S. Al-Dosari and X. Gao, “Nonviral gene delivery: Principle, limitations, and recent Progress,” *AAPS Journal*, vol. 11, no. 4. pp. 671–681, Dec. 2009. doi: 10.1208/s12248-009-9143-y.

[51] J. Roacho-Perez, H. Gallardo-Blanco, M. Sanchez-Dominguez, P. Garcia-Casillas, C. Chapa-Gonzalez, and C. Sanchez-Dominguez, “Nanoparticles for death-induced gene therapy in cancer (Review),” *Mol Med Rep*, vol. 17, no. 1, pp. 1413–1420, Nov. 2017, doi: 10.3892/mmr.2017.8091.

[52] D. W. Hobson, “Nanotechnology,” in *Comprehensive Biotechnology*, vol. 3, Elsevier, 2011, pp. 683–697. doi: 10.1016/B978-0-08-088504-9.00228-2.

[53] G. Adamo, S. Campora, and G. Ghersi, “Chapter 3 - Functionalization of nanoparticles in specific targeting and mechanism release,” 2017. doi: 10.1016/B978-0-323-46142-9/00003-7.

[54] I. Khan, K. Saeed, and I. Khan, “Nanoparticles: Properties, applications and toxicities,” *Arabian Journal of Chemistry*, vol. 12, no. 7. Elsevier B.V., pp. 908–931, Nov. 01, 2019. doi: 10.1016/j.arabjc.2017.05.011.

[55] E. C. Wang and A. Z. Wang, “Nanoparticles and their applications in cell and molecular biology,” *Integrative Biology (United Kingdom)*, vol. 6, no. 1. pp. 9–26, Jan. 2014. doi: 10.1039/c3ib40165k.

[56] A. Z. Wilczewska, K. Niemirowicz, K. H. Markiewicz, and H. Car, “Nanoparticles as drug delivery systems,” *Pharmacological Reports*, vol. 64, no. 5. Elsevier B.V., pp. 1020–1037, 2012. doi: 10.1016/S1734-1140(12)70901-5.

[57] C. Medina, M. J. Santos-Martinez, A. Radomski, O. I. Corrigan, and M. W. Radomski, “Nanoparticles: Pharmacological and toxicological significance,” *British Journal of Pharmacology*, vol. 150, no. 5. pp. 552–558, Mar. 2007. doi: 10.1038/sj.bjp.0707130.

[58] P. Zhou, W. Liu, Y. Cheng, and D. Qian, “Nanoparticle-based applications for cervical cancer treatment in drug delivery, gene editing, and therapeutic cancer vaccines,” *Wiley Interdisciplinary Reviews: Nanomedicine and Nanobiotechnology*, vol. 13, no. 5. John Wiley and Sons Inc, Sep. 01, 2021. doi: 10.1002/wnan.1718.

[59] H. C. Huang, S. Barua, G. Sharma, S. K. Dey, and K. Rege, “Inorganic nanoparticles for cancer imaging and therapy,” *Journal of Controlled Release*, vol. 155, no. 3. pp. 344–357, Nov. 07, 2011. doi: 10.1016/j.jconrel.2011.06.004.

[60] A. P. Tiwari and S. S. Rohiwal, “Synthesis and Bioconjugation of Hybrid Nanostructures for Biomedical Applications,” in *Hybrid Nanostructures for Cancer Theranostics*, Elsevier, 2019, pp. 17–41. doi: 10.1016/B978-0-12-813906-6.00002-0.

[61] C. Li, J. Wang, Y. Wang, H. Gao, G. Wei, Y. Huang, H. Yu, Y. Gan, Y. Wang, L. Mei, H. Chen, H. Hu, Z. Zhang and Y. Jin, “Recent progress in drug delivery,” *Acta Pharmaceutica Sinica B*, vol. 9, no. 6. Chinese Academy of Medical Sciences, pp. 1145–1162, Nov. 01, 2019. doi: 10.1016/j.apsb.2019.08.003.

[62] D. Huang, B. He, and P. Mi, “Calcium phosphate nanocarriers for drug delivery to tumors: imaging, therapy and theranostics,” *Biomater Sci*, vol. 7, no. 10, pp. 3942–3960, Oct. 2019, doi: 10.1039/C9BM00831D.

[63] R. Khalifehzadeh and H. Arami, “Biodegradable calcium phosphate nanoparticles for cancer therapy,” *Adv Colloid Interface Sci*, vol. 279, p. 102157, 2020, doi: 10.1016/j.cis.2020.102157.

[64] S. Van Rijt, K. De Groot, and S. C. G. Leeuwenburgh, “Calcium Phosphate and Silicate-Based Nanoparticles: History and Emerging Trends,” *Tissue Engineering - Part A*, vol. 28, no. 11–12. Mary Ann Liebert Inc., pp. 461–477, Jun. 01, 2022. doi: 10.1089/ten.tea.2021.0218.

[65] Z. Sun, W. Li, J.C. Lenzo, J.E. Holden, M.E. McCullough, A.M. O’Connor and N.M. O’Brien-Simpson, “The Potential of Calcium Phosphate Nanoparticles as Adjuvants and Vaccine Delivery Vehicles,” *Front Mater*, vol. 8, no. December, pp. 1–17, 2021, doi: 10.3389/fmats.2021.788373.

[66] M. Sadat-Shojai, M. T. Khorasani, E. Dinpanah-Khoshdargi, and A. Jamshidi, “Synthesis methods for nanosized hydroxyapatite with diverse structures,” *Acta Biomaterialia*, vol. 9, no. 8. Elsevier Ltd, pp. 7591–7621, 2013. doi: 10.1016/j.actbio.2013.04.012.

[67] X. Chen, H. Li, Y. Ma, and Y. Jiang, “Calcium Phosphate-Based Nanomaterials: Preparation, Multifunction, and Application for Bone Tissue Engineering,” *Molecules*, vol. 28, no. 12, p. 4790, Jun. 2023, doi: 10.3390/molecules28124790.

[68] L. Degli Esposti, A. Dotti, A. Adamiano, C. Fabbi, E. Quarta, P. Colombo, D. Catalucci, C. De Luca and M. Iafisco, “Calcium phosphate nanoparticle precipitation by a continuous flow process: A design of an experiment approach,” *Crystals (Basel)*, vol. 10, no. 10, pp. 1–17, 2020, doi: 10.3390/cryst10100953.

[69] V. Sokolova and M. Epple, “Biological and Medical Applications of Calcium Phosphate Nanoparticles,” *Chemistry - A European Journal*, vol. 27, no. 27. John Wiley and Sons Inc, pp. 7471–7488, May 12, 2021. doi: 10.1002/chem.202005257.

[70] S. C. J. Loo, T. Moore, B. Banik, and F. Alexis, “Biomedical Applications of Hydroxyapatite Nanoparticles †,” 2010.

[71] M. N. Hassan, M. M. Mahmoud, A. A. El-Fattah, and S. Kandil, “Microwave-assisted preparation of Nano-hydroxyapatite for bone substitutes,” *Ceramics*

International, vol. 42, no. 3. Elsevier Ltd, pp. 3725–3744, Feb. 15, 2016. doi: 10.1016/j.ceramint.2015.11.044.

[72] S. Utara and J. Klinkaewnarong, "Sonochemical synthesis of nano-hydroxyapatite using natural rubber latex as a templating agent," *Ceram Int*, vol. 41, no. 10, pp. 14860–14867, Jun. 2015, doi: 10.1016/j.ceramint.2015.08.018.

[73] Y. Hong, H. Fan, B. Li, B. Guo, M. Liu, and X. Zhang, "Fabrication, biological effects, and medical applications of calcium phosphate nanoceramics," in *Materials Science and Engineering R: Reports*, Nov. 2010, pp. 225–242. doi: 10.1016/j.mser.2010.06.010.

[74] C. Qi, Y.-J. Zhu, G.-J. Ding, J. Wu, and F. Chen, "Solvothermal synthesis of hydroxyapatite nanostructures with various morphologies using adenosine 5′-monophosphate sodium salt as an organic phosphorus source," *RSC Adv*, vol. 5, no. 5, pp. 3792–3798, 2015, doi: 10.1039/C4RA13151G.

[75] T. J. Levingstone, S. Herbaj, and N. J. Dunne, "Calcium Phosphate Nanoparticles for Therapeutic Applications in Bone Regeneration," *Nanomaterials*, vol. 9, no. 11, p. 1570, Nov. 2019, doi: 10.3390/nano9111570.

[76] A. Laskus and J. Kolmas, "Ionic Substitutions in Non-Apatitic Calcium Phosphates," *Int J Mol Sci*, vol. 18, no. 12, p. 2542, Nov. 2017, doi: 10.3390/ijms18122542.

[77] S. Bose and S. Tarafder, "Calcium phosphate ceramic systems in growth factor and drug delivery for bone tissue engineering: A review," *Acta Biomater*, vol. 8, no. 4, pp. 1401–1421, Apr. 2012, doi: 10.1016/j.actbio.2011.11.017.

[78] S. V. Dorozhkin, "Nanosized and nanocrystalline calcium orthophosphates," *Acta Biomater*, vol. 6, no. 3, pp. 715–734, Mar. 2010, doi: 10.1016/j.actbio.2009.10.031.

[79] R. Z. Legeros, "Review paper Biod.egradation and Bioresorption of Calcium. Phosphate Ceramics," 1993.

[80] M. Canillas, P. Pena, A. H. de Aza, and M. A. Rodríguez, "Calcium phosphates for biomedical applications," *Boletín de la Sociedad Española de Cerámica y Vidrio*, vol. 56, no. 3, pp. 91–112, May 2017, doi: 10.1016/j.bsecv.2017.05.001.

[81] W. Habraken, P. Habibovic, M. Epple, and M. Bohner, "Calcium phosphates in biomedical applications: materials for the future?," *Materials Today*, vol. 19, no. 2, pp. 69–87, Mar. 2016, doi: 10.1016/j.mattod.2015.10.008.

[82] C. Moseke and U. Gbureck, “Tetracalcium phosphate: Synthesis, properties and biomedical applications,” *Acta Biomaterialia*, vol. 6, no. 10. Elsevier Ltd, pp. 3815–3823, 2010. doi: 10.1016/j.actbio.2010.04.020.

[83] Y. Yang and C. Yu, “Advances in silica based nanoparticles for targeted cancer therapy,” *Nanomedicine*, vol. 12, no. 2, pp. 317–332, Feb. 2016, doi: 10.1016/j.nano.2015.10.018.

[84] J. J. Rennick, A. P. R. Johnston, and R. G. Parton, “Key principles and methods for studying the endocytosis of biological and nanoparticle therapeutics,” *Nat Nanotechnol*, vol. 16, no. 3, pp. 266–276, Mar. 2021, doi: 10.1038/s41565-021-00858-8.

[85] S. Behzadi, V. Serpooshan, W. Tao, M.A. Hamaly, M.Y. Alkawareek, E.C. Dreaden, D. Brown, A.M. Alkilany, O.C. Farokhzad and M. Mahmoudi, “Cellular uptake of nanoparticles: journey inside the cell,” *Chem Soc Rev*, vol. 46, no. 14, pp. 4218–4244, Jul. 2017, doi: 10.1039/C6CS00636A.

[86] Y. Piao, Ho Pan Bei, A. Tam, Y. Yang, Q. Zhang, M. Yang and X. Zhao, “Calcium Phosphate Nanoparticle-Based Systems for Therapeutic Delivery,” in *Theranostic Bionanomaterials*, Elsevier, 2019, pp. 147–164. doi: 10.1016/B978-0-12-815341-3.00006-7.

[87] A. Tabaković, M. Kester, and J. H. Adair, “Calcium phosphate-based composite nanoparticles in bioimaging and therapeutic delivery applications,” *WIREs Nanomedicine and Nanobiotechnology*, vol. 4, no. 1, pp. 96–112, Jan. 2012, doi: 10.1002/wnan.163.

[88] P. Kumari, B. Ghosh, and S. Biswas, “Nanocarriers for cancer-targeted drug delivery,” *J Drug Target*, vol. 24, no. 3, pp. 179–191, Mar. 2016, doi: 10.3109/1061186X.2015.1051049.

[89] L. Degli Esposti, F. Carella, A. Adamiano, A. Tampieri, and M. Iafisco, “Calcium phosphate-based nanosystems for advanced targeted nanomedicine,” *Drug Dev Ind Pharm*, vol. 44, no. 8, pp. 1223–1238, Aug. 2018, doi: 10.1080/03639045.2018.1451879.

[90] I. Velikyan, “Radionuclides for Imaging and Therapy in Oncology,” in *Cancer Theranostics*, Elsevier, 2014, pp. 285–325. doi: 10.1016/B978-0-12-407722-5.00017-7.

[91] S. R. Rout, B. Behera, T. K. Maiti, and S. Mohapatra, “Multifunctional magnetic calcium phosphate nanoparticles for targeted platin delivery,” *Dalton Transactions*, vol. 41, no. 35, p. 10777, Sep. 2012, doi: 10.1039/c2dt30984j.

[92] V. Di Mauro, M. Iafisco, N. Salvarani, M. Vacchiano, P. Carullo, G. Ramírez-Rodríguez, T. Patrício, A. Tampieri, M. Miragoli and D. Catalucci, “Bioinspired negatively charged calcium phosphate nanocarriers for cardiac delivery of MicroRNAs,” *Nanomedicine*, vol. 11, no. 8, pp. 891–906, 2016, doi: 10.2217/nnm.16.26.

[93] C. Santos, P. Gomes, J. A. Duarte, M. M. Almeida, M. E. V. Costa, and M. H. Fernandes, “Development of hydroxyapatite nanoparticles loaded with folic acid to induce osteoblastic differentiation,” *Int J Pharm*, vol. 516, no. 1–2, pp. 185–195, Jan. 2017, doi: 10.1016/j.ijpharm.2016.11.035.

[94] I. Roy, S. Mitra, A. Maitra, and S. Mozumdar, “Calcium phosphate nanoparticles as novel non-viral vectors for targeted gene delivery,” *Int J Pharm*, vol. 250, no. 1, pp. 25–33, Jan. 2003, doi: 10.1016/S0378-5173(02)00452-0.

[95] M. A. Khan, V. M. Wu, S. Ghosh, and V. Uskoković, “Gene delivery using calcium phosphate nanoparticles: Optimization of the transfection process and the effects of citrate and poly(l-lysine) as additives.,” *J Colloid Interface Sci*, vol. 471, pp. 48–58, Jun. 2016, doi: 10.1016/j.jcis.2016.03.007.

[96] S. A. A. Rizvi and A. M. Saleh, “Applications of nanoparticle systems in drug delivery technology,” *Saudi Pharmaceutical Journal*, vol. 26, no. 1, pp. 64–70, Jan. 2018, doi: 10.1016/j.jsps.2017.10.012.

[97] E. Fröhlich, “The role of surface charge in cellular uptake and cytotoxicity of medical nanoparticles,” *Int J Nanomedicine*, vol. 7, p. 5577, Nov. 2012, doi: 10.2147/IJN.S36111.

[98] F. Zhao, Y. Zhao, Y. Liu, X. Chang, C. Chen, and Y. Zhao, “Cellular Uptake, Intracellular Trafficking, and Cytotoxicity of Nanomaterials,” *Small*, vol. 7, no. 10, pp. 1322–1337, May 2011, doi: 10.1002/smll.201100001.

[99] V. Sokolova, D. Kozlova, T. Knuschke, J. Buer, A. M. Westendorf, and M. Epple, “Mechanism of the uptake of cationic and anionic calcium phosphate nanoparticles by cells,” *Acta Biomater*, vol. 9, no. 7, pp. 7527–7535, Jul. 2013, doi: 10.1016/j.actbio.2013.02.034.

[100] J. M. Delgado-López, M. Iafisco, I. Rodríguez, A. Tampieri, M. Prat, and J. Gómez-Morales, "Crystallization of bioinspired citrate-functionalized nanoapatite with tailored carbonate content," *Acta Biomater*, vol. 8, no. 9, pp. 3491–3499, Sep. 2012, doi: 10.1016/j.actbio.2012.04.046.

[101] T. Mudalige, H. Qu, D. Van Haute, S. M. Ansar, A. Paredes, and T. Ingle, "Characterization of Nanomaterials," in *Nanomaterials for Food Applications*, Elsevier, 2019, pp. 313–353. doi: 10.1016/B978-0-12-814130-4.00011-7.

[102] T. J. Levingstone, S. Herbaj, J. Redmond, H. O. McCarthy, and N. J. Dunne, "Calcium phosphate nanoparticles-based systems for rnai delivery: Applications in bone tissue regeneration," *Nanomaterials*, vol. 10, no. 1, pp. 5–10, 2020, doi: 10.3390/nano10010146.

[103] T. Albuquerque, R. Faria, Â. Sousa, A. R. Neves, J. A. Queiroz, and D. Costa, "Polymer-peptide ternary systems as a tool to improve the properties of plasmid DNA vectors in gene delivery," *J Mol Liq*, vol. 309, p. 113157, Jul. 2020, doi: 10.1016/j.molliq.2020.113157.

[104] B. Alallam, S. Altahhan, M. Taher, M. H. Mohd Nasir, and A. A. Doolaanea, "Electrosprayed Alginate Nanoparticles as CRISPR Plasmid DNA Delivery Carrier: Preparation, Optimization, and Characterization," *Pharmaceuticals*, vol. 13, no. 8, p. 158, Jul. 2020, doi: 10.3390/ph13080158.

[105] R. Liu, B. K. Kay, S. Jiang, and S. Chen, "Nanoparticle Delivery: Targeting and Nonspecific Binding," *MRS Bull*, vol. 34, no. 6, pp. 432–440, Jun. 2009, doi: 10.1557/mrs2009.119.

[106] F. N. Parin, S. Ullah, K. Yildirim, M. Hashmi, and I.-S. Kim, "Fabrication and Characterization of Electrospun Folic Acid/Hybrid Fibers: In Vitro Controlled Release Study and Cytocompatibility Assays," *Polymers (Basel)*, vol. 13, no. 20, p. 3594, Oct. 2021, doi: 10.3390/polym13203594.

[107] Q. Liu, W. Guo, M. Yang, K. Wang, W. Liu, and F. Wu, "Release Behavior of Folic Acid Grafted Hollow Hydroxyapatite as Drug Carrier," *Advances in Polymer Technology*, vol. 2019, pp. 1–9, Mar. 2019, doi: 10.1155/2019/9562437.

[108] S. Ullah, S. Ferdosh, A. Nawaz, K. Shah, M. Iqbal, G. Albadrani, F. Al-Joufi, A. Sayed, and M. Abdel-Daim, "5-Fluorouracil-Loaded Folic-Acid-Fabricated Chitosan Nanoparticles for Site-Targeted Drug Delivery Cargo," *Polymers (Basel)*, vol. 14, no. 10, May 2022, doi: 10.3390/polym14102010.

[109] S. Bandara, C. Carnegie, C. Johnson, F. Akindoju, E. Williams, J.M. Swaby, A. Oki, and L.E. Carson, "Synthesis and characterization of Zinc/ Chitosan-Folic acid complex," *Heliyon*, vol. 4, p. 737, 2018, doi: 10.1016/j.heliyon.2018.e00737.

[110] S. Yang, F. Lin, K. Tsai, M. Wei, H. Tsai, J. Wong, and M. Shieh, "Folic acid-conjugated chitosan nanoparticles enhanced protoporphyrin IX accumulation in colorectal cancer cells," *Bioconjug Chem*, vol. 21, no. 4, pp. 679–689, Apr. 2010, doi: 10.1021/bc9004798.

[111] B. Lin, H. Chen, D. Liang, W. Lin, X. Qi, H. Liu, and X. Deng, "Acidic pH and High-H_2O_2 Dual Tumor Microenvironment-Responsive Nanocatalytic Graphene Oxide for Cancer Selective Therapy and Recognition," *ACS Appl Mater Interfaces*, vol. 11, no. 12, pp. 11157–11166, Mar. 2019, doi: 10.1021/acsami.8b22487.

[112] S. Jang, S. Lee, H. Kim, J. Ham, J.-H. Seo, Y. Mok, M. Noh, and Y. Lee, "Preparation of pH-sensitive CaP nanoparticles coated with a phosphate-based block copolymer for efficient gene delivery," *Polymer (Guildf)*, vol. 53, no. 21, pp. 4678–4685, Sep. 2012, doi: 10.1016/j.polymer.2012.08.043.

[113] W. Li, X. Zhang, S. Jing, X. Xin, K. Chen, D. Chen, and H. Hu, "Preparation of Calcium Phosphate/pDNA Nanoparticles for Exogenous Gene Delivery by Co-Precipitation Method: Optimization of Formulation Variables Using Box-Behnken Design," *J Pharm Sci*, vol. 106, no. 8, pp. 2053–2059, Aug. 2017, doi: 10.1016/j.xphs.2017.04.049.

[114] S. Bisht, G. Bhakta, S. Mitra, and A. Maitra, "pDNA loaded calcium phosphate nanoparticles: highly efficient non-viral vector for gene delivery," *Int J Pharm*, vol. 288, no. 1, pp. 157–168, Jan. 2005, doi: 10.1016/j.ijpharm.2004.07.035.

[115] V. Kuete, O. Karaosmanoğlu, and H. Sivas, "Anticancer Activities of African Medicinal Spices and Vegetables," in *Medicinal Spices and Vegetables from Africa*, Elsevier, 2017, pp. 271–297. doi: 10.1016/B978-0-12-809286-6.00010-8.

[116] J. López-García, M. Lehocký, P. Humpolíček, and P. Sáha, "HaCaT Keratinocytes Response on Antimicrobial Atelocollagen Substrates: Extent of Cytotoxicity, Cell Viability and Proliferation," *J Funct Biomater*, vol. 5, no. 2, pp. 43–57, May 2014, doi: 10.3390/jfb5020043.

[117] K. Siwowska, R. Schmid, S. Cohrs, R. Schibli, and C. Müller, "Folate Receptor-Positive Gynecological Cancer Cells: In Vitro and In Vivo Characterization," *Pharmaceuticals*, vol. 10, no. 4, p. 72, Aug. 2017, doi: 10.3390/ph10030072.

[118] C. E. Pedraza, D. C. Bassett, M. D. McKee, V. Nelea, U. Gbureck, and J. E. Barralet, “The importance of particle size and DNA condensation salt for calcium phosphate nanoparticle transfection,” *Biomaterials*, vol. 29, no. 23, pp. 3384–3392, Aug. 2008, doi: 10.1016/j.biomaterials.2008.04.043.

[119] V. Sokolova, L. Rojas-Sánchez, N. Białas, N. Schulze, and M. Epple, “Calcium phosphate nanoparticle-mediated transfection in 2D and 3D mono- and co-culture cell models,” *Acta Biomater*, vol. 84, pp. 391–401, Jan. 2019, doi: 10.1016/j.actbio.2018.11.051.